DTIC FILE COPY

AD-A217 443

DOCUMENTATION PAGE

Form Approved
OMB No. 0704-0188

1b. RESTRICTIVE MARKINGS
NONE

2. SECURITY CLASSIFICATION AUTHORITY

3. DISTRIBUTION/AVAILABILITY OF REPORT
APPROVED FOR PUBLIC RELEASE;
DISTRIBUTION UNLIMITED.

2b. DECLASSIFICATION/DOWNGRADING SCHEDULE

4. PERFORMING ORGANIZATION REPORT NUMBER(S)

5. MONITORING ORGANIZATION REPORT NUMBER(S)
AFIT/CI/CIA-89-038

6a. NAME OF PERFORMING ORGANIZATION
AFIT STUDENT AT NORTH CAROLINA STATE UNIVERSITY

6b. OFFICE SYMBOL (If applicable)

7a. NAME OF MONITORING ORGANIZATION
AFIT/CIA

6c. ADDRESS (City, State, and ZIP Code)

7b. ADDRESS (City, State, and ZIP Code)
Wright-Patterson AFB OH 45433-6583

8a. NAME OF FUNDING/SPONSORING ORGANIZATION

8b. OFFICE SYMBOL (If applicable)

9. PROCUREMENT INSTRUMENT IDENTIFICATION NUMBER

8c. ADDRESS (City, State, and ZIP Code)

10. SOURCE OF FUNDING NUMBERS

PROGRAM ELEMENT NO.	PROJECT NO.	TASK NO.	WORK UNIT ACCESSION NO.

11. TITLE (Include Security Classification) (UNCLASSIFIED)
Inland Evolution of the Coastal Front During IOP-2, 25 January 1986

12. PERSONAL AUTHOR(S)
John M. Egentowich

13a. TYPE OF REPORT	13b. TIME COVERED	14. DATE OF REPORT (Year, Month, Day)	15. PAGE COUNT
THESIS/DISSERTATION	FROM _____ TO _____	1989	92

16. SUPPLEMENTARY NOTATION
APPROVED FOR PUBLIC RELEASE IAW AFR 190-1
ERNEST A. HAYGOOD, 1st Lt, USAF
Executive Officer, Civilian Institution Programs

17. COSATI CODES		
FIELD	GROUP	SUB-GROUP

18. SUBJECT TERMS (Continue on reverse if necessary and identify by block number)

19. ABSTRACT (Continue on reverse if necessary and identify by block number)

DTIC
ELECTE
FEB 01 1990
S D
E

90 02 01 015

20. DISTRIBUTION/AVAILABILITY OF ABSTRACT
☒ UNCLASSIFIED/UNLIMITED ☐ SAME AS RPT. ☐ DTIC USERS

21. ABSTRACT SECURITY CLASSIFICATION
UNCLASSIFIED

22a. NAME OF RESPONSIBLE INDIVIDUAL	22b. TELEPHONE (Include Area Code)	22c. OFFICE SYMBOL
ERNEST A. HAYGOOD, 1st Lt, USAF	(513) 255-2259	AFIT/CI

DD Form 1473, JUN 86 Previous editions are obsolete. SECURITY CLASSIFICATION OF THIS PAGE

AFIT/CI "OVERPRINT"

Inland Evolution Of The Coastal Front During IOP-2, 25 January 1986

by

John M. Egentowich

A thesis submitted to the Graduate Faculty of
North Carolina State University
in partial fulfillment of the
requirements for the Degree of
Master of Science

Department of Marine, Earth, and Atmospheric Sciences

Raleigh
1989

Approved By:

Chairman of Advisory Committee

Abstract

EGENTOWICH, JOHN M. Inland Evolution Of The Coastal Front During IOP-2, 25 January 1986 (Under the direction of Allen J. Riordan).

A unique case of mid-Atlantic coastal frontogenesis on 25 January 1986 is examined through mesoscale analysis to illustrate various stages of it's evolution. This analysis suggests that as the coastal front moves onshore and passes over Pamlico Sound in eastern North Carolina, the front breaks down to form two separate boundaries. The inland boundary is characterized by a strong temperature gradient, while a second weaker front remains along the coast. The Barnes analysis scheme is applied to data from the PAM network to obtain wind fields and areas of convergence. Two identifiable areas of convergence are associated with the two fronts.

The importance of vertical mixing is examined and a numerical finite-difference scheme is used to evaluate the magnitude of individual terms of the frontogenesis equation. Lastly, an error analysis is performed to determine the level of reliability of the frontogenesis analysis.

Keywords: Thesis, Case Study, GALE project, GALE (Genesis of Atlantic Lows Experiment), (KR)

Table of Contents

1. INTRODUCTION

1.1 Introduction

Coastal fronts in the United States are mesoscale features confined to eastern coastal regions. They typically form as a boundary between a light northerly flow (5m/s) of cold air and a stronger (10m/s) easterly maritime air flow. The effects of orography, coastal configuration, land-sea temperature contrast, and friction play a major role in the formation, intensification, and dissipation of these coastal fronts. Formed mostly in the winter months, these phenomena are characterized by cyclonic wind shifts and have many of the characteristics of warm fronts.

Coastal fronts are very shallow systems and develop quickly, so they present many problems to the local forecaster. These problems include the development of unexpected precipitation (whether in the form of rain, freezing rain, or snow) and large fluctuations in temperature as the front traverses coastal locations. Still another forecasting problem is that coastal fronts often become sites of cyclogenesis, a few of which develop into strong systems that track northward along the east coast. The greatest difficulty is that the numerical models generally tend to smooth out this small-scale phenomenon. Thus, the forecaster is hampered in predicting both the

local and larger scale effects of the coastal front.

Coastal fronts form in only a few locations along the east coast because of the local geography. Bosart (1975) observed that the coastline must be curved anticyclonically as viewed from north to south. Thus, the coastal front is confined to the New England, southeast, and occasionally the Texas coast. This geographical preference is due to the fact that the anticyclonically curved coastal areas produce a favorable axis of dilatation for the observed wind which is often aligned parallel to the isotherms. Simultaneously, an axis of pronounced convergence at the surface becomes oriented across these coastal areas.

Synoptically, the most important features for the formation of a coastal front are the presence of a cold anticyclone centered to the north, for example, over northern New England and an upper air wave disturbance located in the midwest (Ballentine, 1980). This anticyclone in northern New England results in a northerly flow along the Piedmont east of the Appalachians. A southward funneling of cold air creates a narrow inverted pressure ridge as the shallow pool of cold air is trapped between the mountains and the coast. As the upper-level wave disturbance then approaches the east coast, it strengthens the southward pressure gradient, thus strengthening the easterly flow over the ocean.

The air over the ocean is modified by the warm waters of the Gulf Stream. Here air of mid-troposphere or continental origin

warms and moistens from fluxes of sensible and latent heat. As the flow over the ocean becomes easterly the warmer air moves back toward the land. Thus, a sharpening boundary is created between the warmer ocean air and the cold air trapped east of the mountains.

1.2 Literature Review

1.2.1 Frontogenesis

Frontal systems were first recognized by Bjerknes (1919) as significant features of the atmosphere. His analyses of fronts were based upon study of a dense network of surface reporting stations. Fronts were first considered as intersections on the earth's surface of sloping surfaces of different densities. He believed the discontinuity existed well into the troposphere.

Several years later there were sufficient soundings to study the three-dimensional aspects of the frontal structure. Some of the first three-dimensional studies were completed by Bjerknes (1932) and Bjerknes and Palmen (1937). As frontal boundaries were identified in the upper levels, they appeared to be first-order discontinuities with respect to density. There was a sharp contrast in the temperature gradient, but not a sharp temperature change. This observation lead to the theory that fronts are thermal transition zones.

After the elementary characteristics of frontal zones were examined, one avenue of exploration was to investigate the associated frontogenesis. Petterssen (1940) defined frontogenesis, in the Eulerian system,as:

$$F = \frac{\partial |\nabla S|}{\partial t},$$

where S is a scalar quantity, usually temperature, and has a continuous distribution in the horizontal plane. Frontogenesis is occurring if the S-isopleths move in such a way that they create a second-order discontinuity along a continuous, stationary or moving, curved or nearly linear locus of points. Frontogenesis occurs where F reaches a local maximum on any line, which means that the magnitude of the gradient of S must increase more rapidly along the line of frontogenesis than either side of this line.

From fluid kinematics it is known that the linear field of motion is divided into four elementary fields: translatory, deformative, divergent, and rotational. No frontogenesis or frontolysis is possible in the translatory field because the velocity is constant, so all the distances between the air parcels are preserved. The deformative field is frontogenetic when the angle between the S-isopleths (isotherms) and the axis of dilatation is less than 45°; it is frontolytic when the angle is larger than 45°. The field of convergence is always frontogenetical and the field of divergence is always frontolytical. The rotational field is neither frontogenetical or frontolytical.

The concept of frontogenesis was commonly restricted to the *earth's surface where the vertical motion is zero, except for upslope* and downslope motion along sloping terrain. Miller (1948) restated the three-dimensional frontogenetic function as parcel following:

$$F_3 = \frac{d|\nabla S|}{dt}.$$

The increase in the number of upper-air observations allowed the analysis of upper-level fronts, thus upper-air analysis of frontogenesis.

There are different factors that affect frontogenesis at different levels, Newton (1954) performed a case study and calculated the relative importance of each. Near the earth's surface and near the maximum wind level, divergence and thermal advection were found to be the dominant factors to frontogenesis. In the mid-levels, vertical motion was the most important. Throughout all levels the vertical variations in ageostrophic wind components normal to the wind direction were significant in producing changes in the vertical shear and stability. Also, the confluence mechanism in the middle troposphere accounted for a necessary part of the concentration of the temperature field (Namias and Clapp, 1949) .

Frontogenetic models by Hoskins and Bretherton (1972) expanded and mathematically solved factors important for frontogenesis. They listed eight processes or mechanisms that are important in the changing of temperature gradients and, thus, in the formation of fronts: (i) horizontal deformation, (ii) horizontal shearing, (iii) vertical deformation, (iv) differential latent-heat release, (v) differential surface friction, (vi) differential vertical motion, (vii)

turbulence and mixing, and (viii) differential radiation absorption or emission. The frontogenetic equation used for the calculations in this paper accounts for many of the above mechanisms.

Haltiner and Martin (1957) expanded Miller's original three-dimensional equation into:

$$F_3 = \nabla_3 \frac{dS}{dt} - \left(\frac{\partial S}{\partial x} \nabla_3 u + \frac{\partial S}{\partial y} \nabla_3 v + \frac{\partial S}{\partial z} \nabla_3 w \right).$$

If the x-axis is chosen parallel to the front, the y-axis (positive toward warmer air) equation becomes (Palmen and Newton, 1969):

$$F_y = \frac{\partial}{\partial y}\left(\frac{dS}{dt}\right) - \left(\frac{\partial S}{\partial x}\frac{\partial u}{\partial y} + \frac{\partial S}{\partial y}\frac{\partial v}{\partial y} + \frac{\partial S}{\partial z}\frac{\partial w}{\partial y} \right).$$

The first term is the differential diabatic heating contribution, if S is temperature, and includes latent heat release. The second term measures the shear contribution. The third term measures the confluence contribution. The forth term includes the effects of differential vertical motion.

1.2.2 Coastal Frontogenesis

The coastal front was first recognized by Carson (1950) who referred to it as the Gulf Stream Front. Previously, George (1939)

observed that stratus often formed in the winter on the northeast coast when a cold high pressure center was located north of 37° latitude. Carson explained the formation of stratus as follows: The high pressure centered in the eastern United States causes a flow of cold air along the Atlantic Coastal Plain, with a cold wedge between the mountains and the coast. Because of the heating and pressure drop over the ocean, the ridge of high pressure becomes positioned north and west of the Gulf Stream. With these conditions, an inverted trough forms east of the ridge. The air over the Gulf Stream is heated by the ocean where an easterly current carries it back over land. Since the depth of this warm air is generally less than 1000 feet, condensation creates low-level stratus. Also, there was very little precipitation associated with the Gulf Stream Front.

Bosart (1972) was one of the first to study the mesoscale features that form along the New England coast and refer to them as coastal fronts. Again, the coastal front was seen as a boundary between the cold northerly flow and the warm easterly maritime flow off the Atlantic. The general New England coastal front was characterized by a 10°C temperature contrast over 5-10 km on a length scale of 100 km, cyclonic wind shifts, and a low-level structure similar to a warm front. Also, the boundary was often the dividing line between frozen and non-frozen precipitation. The front tended to form 12 hours in advance of the passage of coastal low pressure centers.

According to Bosart (1972), surface friction, especially large over the mountains and hilly terrain of New England, creates a large component of cross-isobar flow over land. With a low pressure trough near the coast, this ageostrophic component was found to strengthen the surface convergence zone and upward motion near the shoreline along the southern portion of New England. Surface vorticity is generated and the thermal contrast is strengthened by the persistent northerly flow. So, it appears that the coastal front formed locally near shore rather than propagating westward from the ocean.

With emphasis on the synoptics and dynamics of formation, Bosart (1975) then studied the coastal front on the basis of individual and climatological case studies. The first observed feature was that a coastal front formed in regions where the coastline curves anticyclonically as viewed north to south. Also, coastal frontogenesis was found to be primarily a cold-season phenomenon.

To study the dynamics, Bosart preformed a case study and calculated the deformation, divergence, and vorticity at the onset of coastal frontogenesis. Most noticeable was the fact that the axis of maximum geostrophic deformation (divergence) was inland. The observed deformation (convergence) was orientated north-south from Boston to Providence and was strongest offshore. Also, there appeared no well defined area of relative vorticity, but there was a

hint of cyclonic flow north of Cape Cod.

The distribution of precipitation near the coastal front relative to New England storm systems is another important aspect first studied by Marks and Austin (1977). Again, the front was observed to be a low-level phenomenon typically occurring well ahead of the surface cyclone and synoptic scale surface warm front. The precipitation that fell in the vicinity of the coastal front resulted mainly from the large-scale circulation. The precipitation developed from the warm, moist, southerly flow above the coastal front. Thus, the coastal front did not create new areas of precipitation; rather, it produced local intensification. The typical amounts of intensification appeared to be between 20% and 50%.

Richwien (1980) investigated the damming effect of the southern Appalachians. The first aspect studied of the mountain damming was how the numerical models were forecasting the event. The models consistently missed the damming and forecast the surface pressure to the east of the Appalachians 4 mb too low. In addition, the forecast and actual wind fields differed by as much as 180° and the wind speeds differed by as much as 30 m/s. Schwerdtfeger (1973) concluded that "the streamlines of a shallow, stable airmass near the ground flowing toward a mountain barrier are deflected to the left over the slopes of the obstacle. The change of direction becomes more pronounced as the temperature inversion (from the cold air nearest the ground to the warmer air aloft) becomes

stronger." In addition, the reduction to sea-level pressure and the resulting pressure field are incorrect because of the inversion and sloping terrain. Also, Bosart (1972) observed that coastal fronts persist parallel to the terrain contours and not to the coastline. So, the mountain-damming apparently plays an important role in the formation of the coastal fronts.

Ballentine (1980) preformed an in-depth numerical investigation of the New England coastal frontogenesis. His investigation studied the effects of latent heat release, land-sea temperature contrast, synoptic-scale forcing, surface friction, irregular coastline, and irregular terrain. The first experiment was called the basic experiment because all the important physical effects were included. Each successive experiment removed one important physical effect of the frontogenesis. The results showed that a synoptic-scale wave disturbance at 700 mb is a necessary but not sufficient condition for the development of a strong coastal front circulation. Also, through thermally-induced circulation, the heat fluxes from the ocean are primarily responsible for the convergence along the coast. Finally, differential friction, orography, and latent heat release are of secondary importance.

Another coastal front case was studied when it formed along the East Coast associated with the President's Day snowstorm. Bosart (1981) and Bosart and Lin (1984) performed extensive research on this coastal front development. During its initial development,

Bosart found that the front is strongly frontogenetic below 950 mb and frontolytic above 950 mb, a finding which reinforces the concept of a very low-level phenomenon.

In a brief study of the marine boundary layer near a coastal front, Riordan et. al. (1985) computed the latent and sensible heat fluxes. They characterized the coastal front as a division between the warm, moist air (with large heat fluxes) and cooler, stable air (negligible heat fluxes). They also found that coastal fronts that are undetected in routine analysis may be important in fostering small weather disturbances.

1.3 Research Goals/Objectives

Coastal fronts are very shallow systems and develop quickly so they present many problems to the local forecaster. These problems include the development of unexpected precipitation and large changes in temperature as the front traverses coastal areas. Another problem is that coastal fronts often become sites of cyclogenesis. The greatest problem is that computer models tend to smooth over these small disturbances so the local forecaster has little advance warning of the coastal fronts.

The goals of the present research are to employ the enhanced-resolution data set collected during the Genesis of Atlantic Lows Experiment (GALE) to:

i) produce a mesoscale analysis of various stages on the evolution of a coastal front in the Carolinas on 25 January 1986

ii) follow and explain the development of the coastal front by a numerical finite-difference evaluation of the individual terms

iii) obtain an error estimate for the frontogenetic terms.

1.4 GALE Project

The field phase of the GALE project was conducted from 15 January to 15 March 1986. The objectives of GALE were to study mesoscale precipitation and air-sea interaction processes in East Coast winter storms, with their particular contributions to cyclogenesis (Dirks et al., 1988). To accomplish these objectives, the research described in this thesis deals primarily with a case study of the evolution of a coastal front on 25 January 1986 [Intensive Observing Period (IOP) 2]. This case was chosen because it presents a unique opportunity to study the synoptic and mesoscale features associated with the development of the coastal front.

The GALE observing systems consisted of soundings, surface measurements, observations from ships, aircraft, radar, and satellite systems. They are described in the next section.

2. CASE STUDY DATA AND METHODOLOGY

2.1 Data Collection

The data for this research were a combination of standard observations and special observations at National Weather Service (NWS) and military stations, and at supplemental sites operated specifically for the GALE field program.

There were two data-gathering areas of particular significance to the present research:

a) Inner GALE Area

The Inner GALE Area was approximately 500-km wide, centered on the coast, and extended 1000km from Georgia to Virginia (Fig.2.1). In this area the meso-β processes of frontogenesis and the coastal front evolution will be examined. Portable-Automated-Mesonet (PAM II), Doppler radars, ships, buoys, most aircraft flights and the Cross-chain Loran Atmospheric Sounding System (CLASS) rawinsonde sites were in this area.

b) Regional GALE Area

The Regional GALE Area was 1,000-km wide (from the ridge of the Appalachians to 500-km offshore), and 1,500-km long (from Florida to New Jersey; see Fig. 2.1). The time and space scale for frontogenesis and the coastal front are on the order of 2-24 h and

200-2000 km (Dirks et al., 1988). The regional area will allow meso-α processes of frontogenesis and cyclogenesis to be synoptically examined.

The objectives of GALE require mesoscale analysis, so the data collection network must be intensive. This section concentrates on the observing facilities used in this research.

a) Sounding operations

The GALE sounding operations were designed to provide three-dimensional fields with time resolution adequate to resolve the structure and evolution of mesoscale weather systems in the GALE observational network. The sounding network for GALE consisted of 39 National Weather Service sites which made launches at 3-hour intervals upon request of GALE Operations. Within and near the Regional GALE area, seventeen additional land-based rawinsonde sites participated, as well as systems aboard 2 ships in the Atlantic coastal waters. The additional sites included seven Cross-chain LORAN-C Atmospheric Sounding System (CLASS) sites in North Carolina and South Carolina which launched as frequently as every 90 minutes on certain occasions. GALE dropwindsonde flights off the Carolina coast sought to complement the dense land-based network (Fig. 2.1).

b) Surface measurements

The surface measurements were designed to provide surface data fields of standard meteorological parameters within the Inner GALE Area with mesoscale resolution and to provide a complement to the data gathered through sounding operations. Standard measurements included air temperature, dewpoint temperature, barometric pressure, wind speed, and wind direction. In addition, land-based stations measured precipitation, and sea-based stations measured sea temperature.

The fifty-station PAM-II network (Fig. 2.2) provided automated 5-minute-averaged meteorological surface observations over the eastern half of North Carolina and South Carolina and southeastern Virginia. A line of four stations also extended northwestward to support a sounding cross-section for cold-wedge studies.

Deployment of the eight special GALE buoys, including six North Carolina State University buoys and two NOAA-E buoys (Fig. 2.2), supported studies of the development of the coastal front and augmented observations in the data-sparse oceanic region in the Inner GALE Area.

c) Ships

The oceanographic research vessels R/V Cape Hatteras (RVC) and R/V Endeavor (RVC) during IOP 2 operated off the coast of North and South Carolina. The data recorded were wind speed, wind direction, air temperature, sea temperature, barometric pressure, and

humidity. The two ships also served as launch platforms for soundings, as mentioned above.

d) Aircraft operations

Generic flight tracks for each of the research aircraft were developed for a variety of weather scenarios. These tracks were designed to provide, but were not limited to, *in situ* measurements of mesoscale features and processes in precipitation regions and their enviroments, and measurements of the horizonal and vertical air-motion field.

e) Radar operations

An operational strategy for the GALE radars was to document the three-dimensional distribution of precipitation over the Inner GALE observational area. The standard NWS radar network included 10 radars that provided useful coverage of the Regional and Inner GALE Areas. Five of the above were digitized to produce 5-minute samples. There were two scanning Doppler radars located on the outer banks of North Carolina (Ocracoke and Hatteras Point, North Carolina). They often scanned in the same area simultaneously in order to resolve the horizonal wind field and were frequently synchronized with aircraft missions in the Hatteras area. In addition, there was a Doppler radar operated by MIT and located at Wilmington, North Carolina, which covered the southern coast of

North Carolina, and a long-range Doppler radar (SPANDAR) operated by NASA and located near the north end of the Regional area at Wallops Island, Virginia.

f) Satellite systems

A variety of satellites collected imagery and soundings in the GALE area. Products specifically used in this study include GOES-6 4km resolution infrared and 1km resolution visible imagery and NOAA-9 sea surface temperatures.

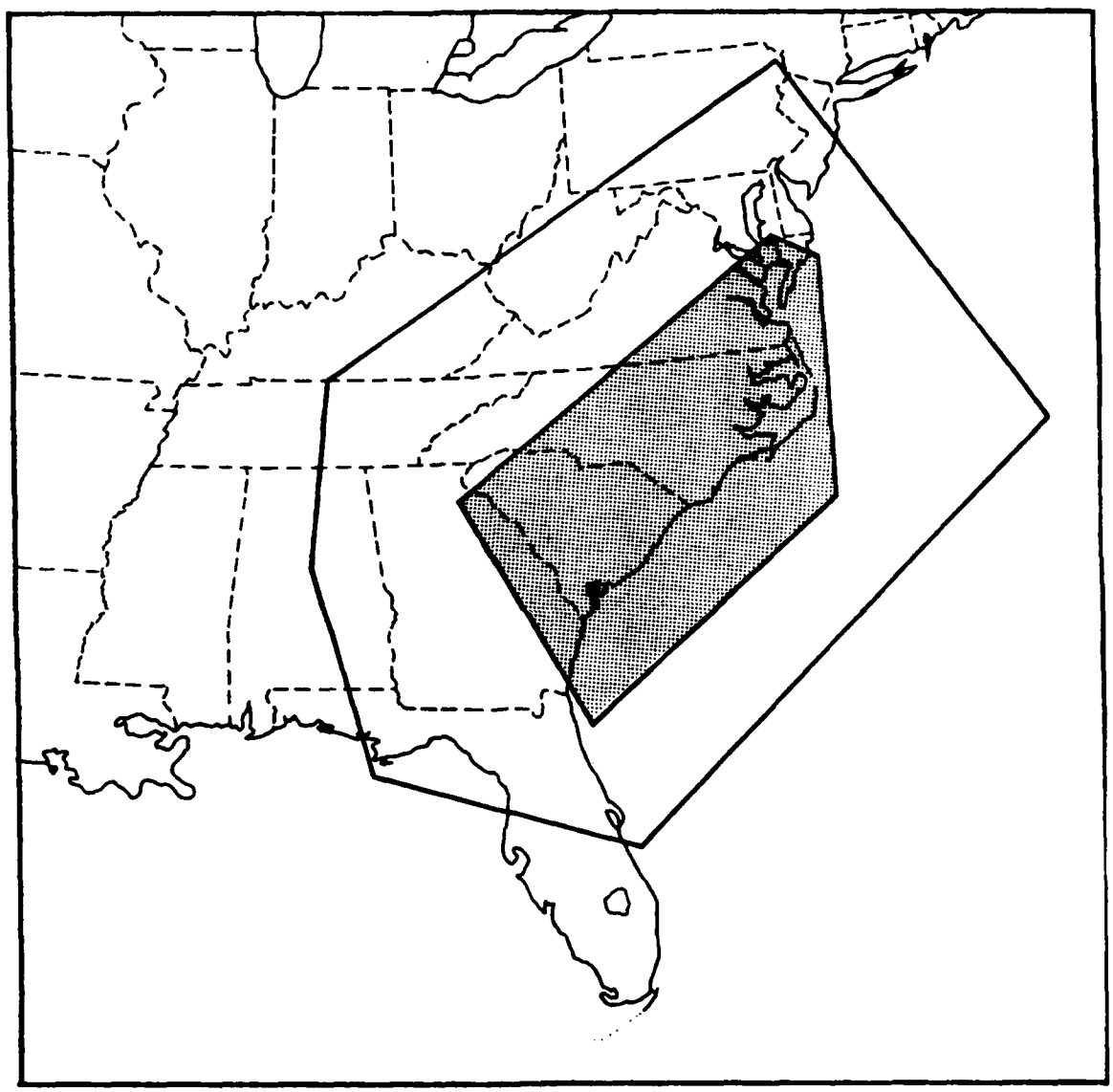

Figure 2.1 - Inner Gale Area (shaded) and Regional GALE Area (outlined).

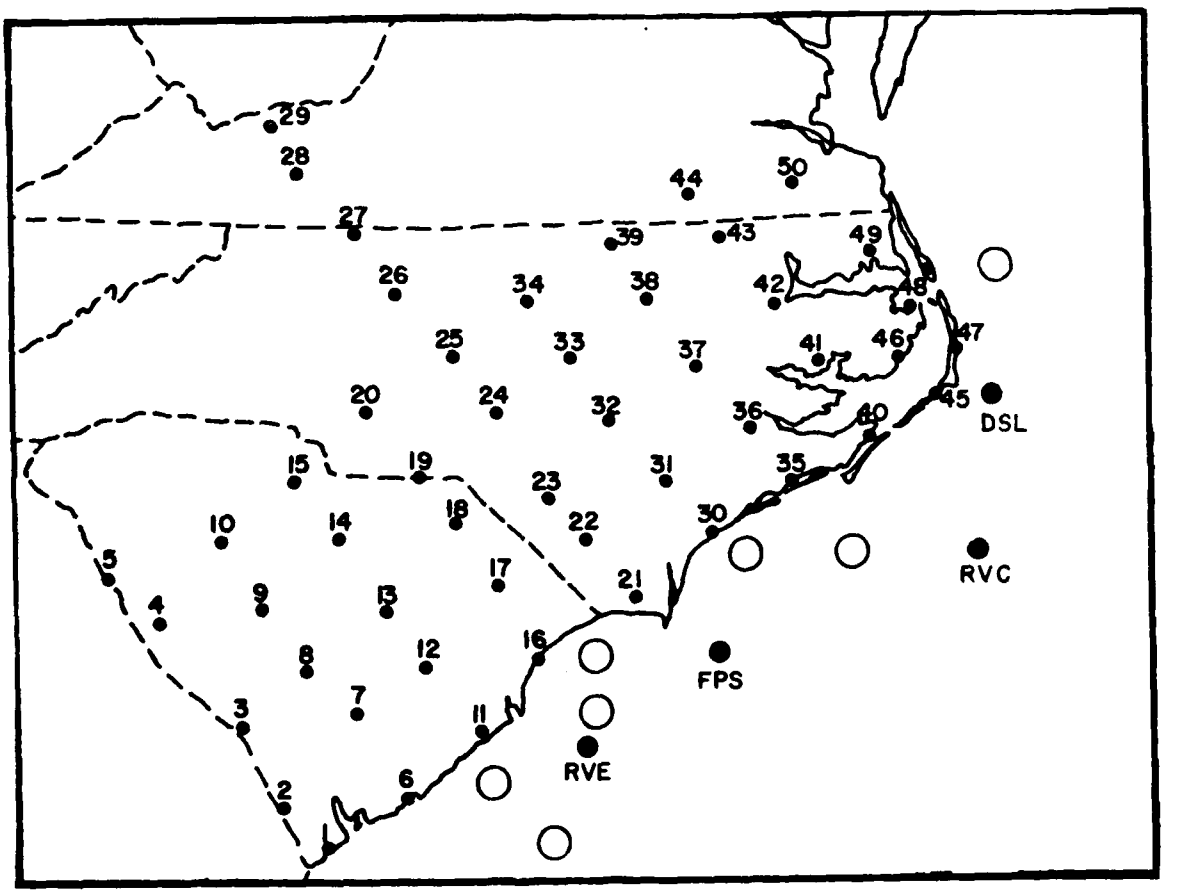

Figure 2.2 - The 50 station PAM-II network, also includes the NCSU buoys, the platforms, and the general location of the ships.

2.2 Barnes Objective Analysis Scheme

The analysis of meteorological fields, especially those to be used in computations, was aided by the Barnes (1964, 1973) objective analysis method. This widely-employed scheme accepts data from observation points and mathematically interpolates to any desired geographical location. In particular, the scheme is used to obtain values at points in a two-dimensional grid array to be used in finite-difference calculations. For example, if q represents any meteorological variable, the interpolated value is just the weighted mean (q) of observations surrounding the point. That is,

$$\overline{q} = \sum_{i=1}^{N} w_i q_i \Big/ \sum_{i=1}^{N} w_i$$

Here, N is the total number of stations "influencing" a given grid point. The observation weights, w, are inverse-distance (d) dependent and are defined by

$$w = \exp(-d^2 / k)$$

Here, k is the weight parameter which controls the rate at which the

weight value decreases outward from the point of interpolation. Hence, k determines the degree of smoothing of the data field. If k is small, there is little smoothing. If k is large, there is greater smoothing.

The selection of k is crucial to the structural detail remaining in the interpolated field. The choice of this parameter value must strike a balance between retaining as much detail as the observation network density allows, and filtering out sub-scale variations and random error. Structural detail is limited by the minimum resolvable wavelength. The GALE PAM-II stations have a mean spacing of about 68 km. This distance is about one-half the normal operational reporting network. Theoretically, the PAM-II can resolve features of twice the mean station separation, or about 140 km.

The weight parameter, k, is selected to reflect the degree of credibility given the amplitudes of the minimally-resolved waves, that is, the signal to noise ratio of the observations at small wavelengths. Sources of "error" include turbulent fluctuations with periods of several minutes (especially near the ground), biases introduced by local topography and obstacles at observation sites (again, especially important for surface stations), and features on scales smaller than the station spacing (e.g. gravity waves). To suppress this noise in the observations a total response of 0.18 in the minimally resolved waves is adopted. This degree of amplitude

suppression is generally consistent with some recent applications of the Barnes scheme, including Barnes (1985) and Moore and Blakley (1988). With a convergence parameter of 0.3, the weight parameter is 2860 km^2. The wind components and temperature are interpolated to a mesh of points with a grid spacing of 40 km (polar stereographic projection, 60°N) or about 34 km at the mean latitude of the PAM-II network.

3. CASE STUDY OF THE EVOLUTION OF A COASTAL FRONT: 25 JANUARY 1986

3.1 Synoptic Overview

3.1.1 Satellite Imagery

Infrared imagery for 1200 UTC 25 January (Fig. 3.1a) depicts widespread cloudiness over the Tennessee and Ohio Valley stretching to the East Coast. Extending northward from Louisiana, there is a comma-shaped area of enhanced cloudiness associated with a surface cyclone and cold front over the Mississippi Valley. Based on comparison with soundings, the cloud shield over North and South Carolina varies in height from 18-20 km along the coast to 28-30 km over the mountains. Three hours later (Fig. 3.1b), most of the Carolinas are overcast, except for small areas of clearing in the south portion of the Pamlico Sound and in the southeastern part of North Carolina. By 1800 UTC 25 January (Fig. 3.1c) an area of clearing has spread southward to the South Carolina coast. There is also a more distinctive boundary between the clouds and the clearing along the coastal areas.

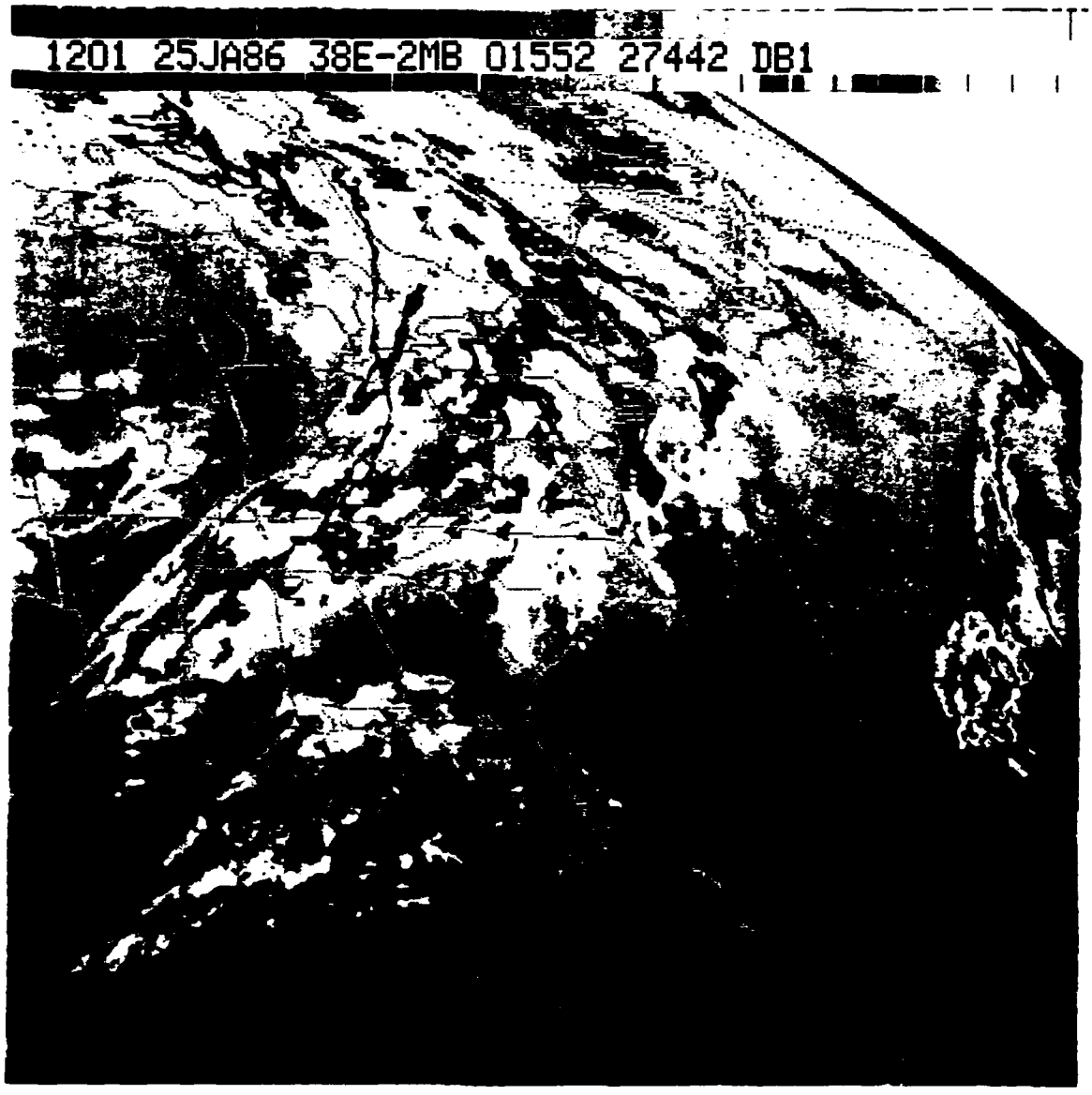

Figure 3.1a - Infrared Satellite Imagery on 25 January 1986 for 1200 UTC.

Figure 3.1b - Infrared Satellite Imagery on 25 January 1986 for 1500 UTC.

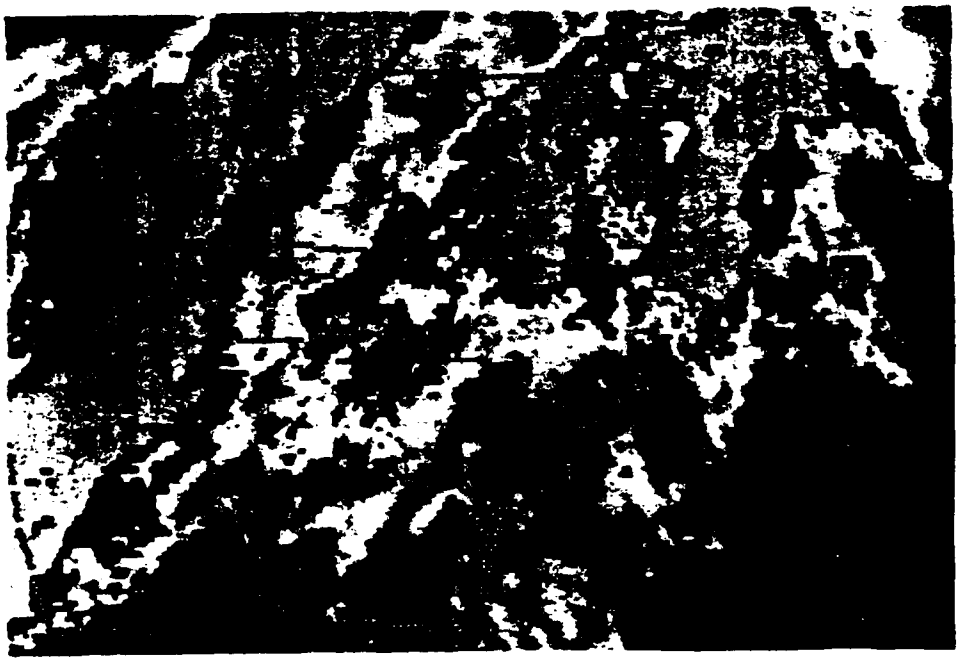

Figure 3.1c - Infrared Satellite Imagery on 25 January 1986 for 1800 UTC.

3.1.2 Upper Air Analysis

The 500-mb analysis (Fig. 3.2a) indicates a deep trough over the Midwest extending southward from Wisconsin to Texas. The flow across the Carolinas is from the west-southwest with little warm-air advection. There is a vorticity maximum located over Wisconsin and Lake Michigan and a secondary maximum located in the base of the trough. However, over North and South Carolina there is little vorticity gradient along the streamlines. The jet core at 300-mb stretches from the base of the trough, in Texas, across the Ohio Valley with a maximum speed of 100 kts. The 700-mb analysis (not shown) depicts southwest flow with accompanying warm-air advection over the Carolinas. The 850-mb analysis (Fig. 3.2b) at 1200 UTC indicates that strong warm-air advection is occurring along the east coast. This warm-air is rising over the cold air trapped on the east side of the Appalachian Mountains.

By 0000 UTC 26 January the trough has moved slightly eastward. The 300-mb flow over the Carolinas has become more southwesterly. The 500-mb flow is also southwesterly with two separate vorticity maxima; one over Michigan and the other over Arkansas. The 700-mb and the 850-mb flow is from the south with strong warm-air advection.

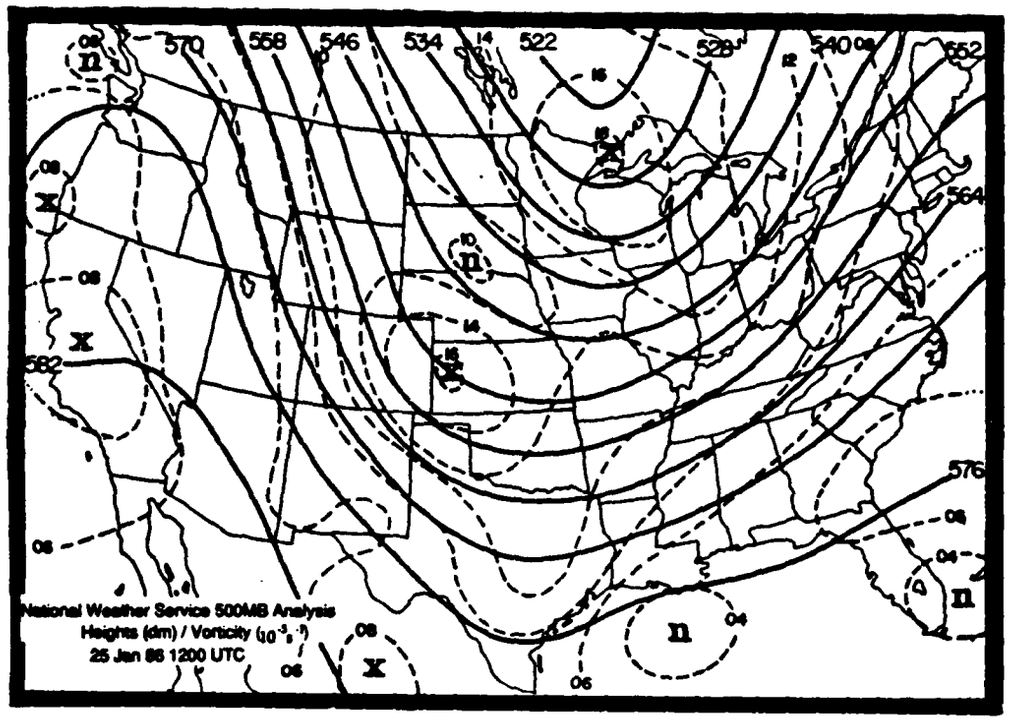

Figure 3.2a - National Weather Service 500MB Analysis for 25 January 1986, Heights (dm) / Vorticity (10^{-5} s^{-1}).

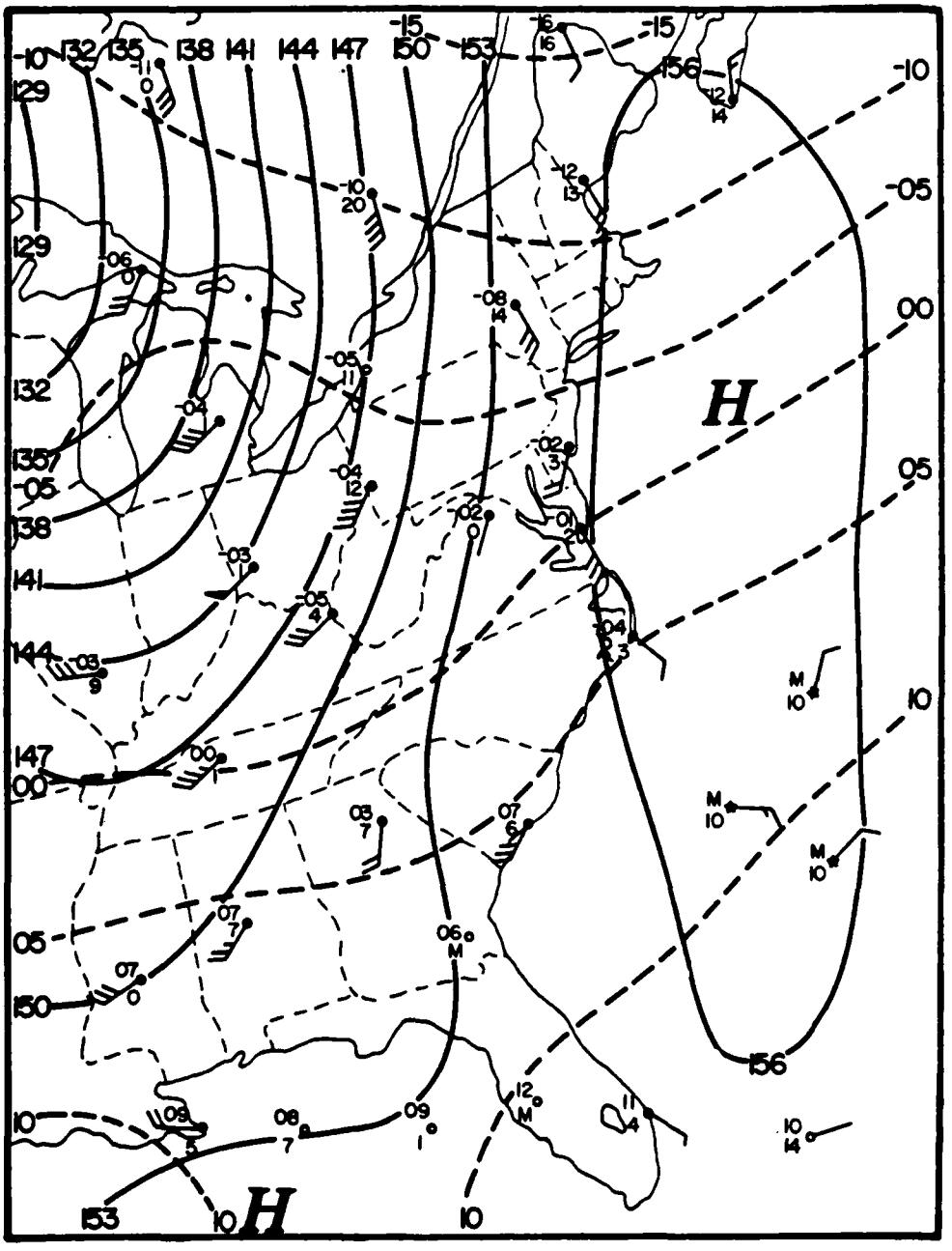

Figure 3.2b - National Weather Service 850MB Analysis on 25 January 1986 for 1200 UTC, Heights (dm) / Isotherms (°C).

3.1.3 Surface Analysis

Figures 3.3a and 3.3b show the NWS surface analysis for 1200 UTC 25 January and for 1800 UTC 25 January. The surface weather conditions for the east coast at 1200 UTC were dominated by a cold anticyclone centered in the Northeast (Maine). The inverted trough along the east coast is evidence of cold-air damming on the east side of the Appalachian Mountains. There is onshore flow along the North Carolina coast, while inland the flow is from the northwest. There is also an area of convergence to the west of the Pamlico Sound with a 100 degree change in wind direction across the trough. The onshore flow and the convergence are associated with an area of scattered rainshowers as seen by radar. The heaviest showers are along the coastal areas. Figure 3.3c depicts the 6-hour total precipitation measured at the PAM sites.

By 1800 UTC the center of the cold anticyclone has moved into Canada. The inverted trough has become more pronounced and moved further inland. The area of convergence is much sharper and is characterized by winds which differ by about 180 degrees across the trough. By this time, the NWS has depicted the trough to be an area of frontogenesis. Also, the rainshowers remain along the coastal region well east of the area of frontogenesis. The detailed analysis of this coastal front will be a main objective of this thesis.

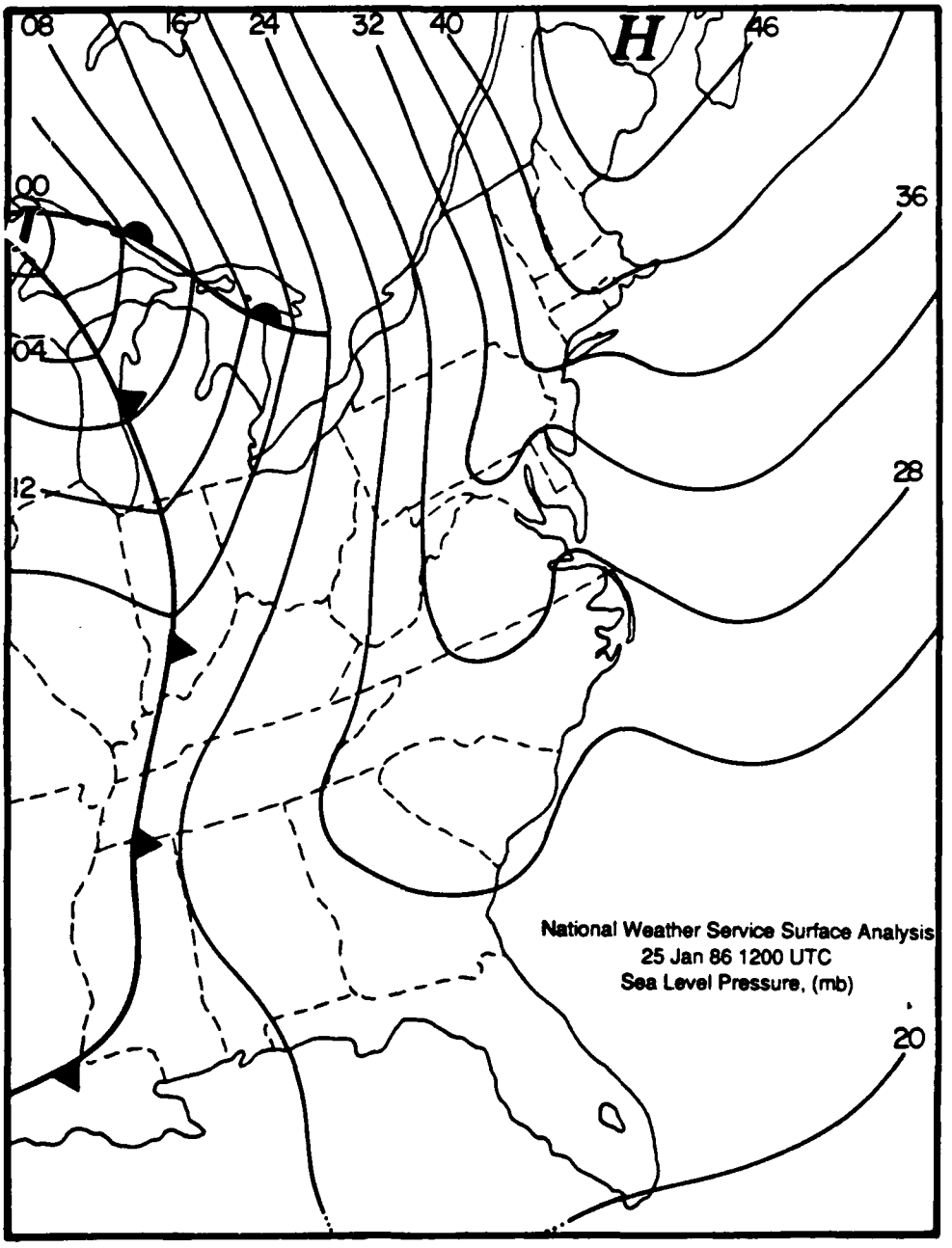

Figure 3.3a - National Weather Service Surface Analysis on 25 January 1986 for 1200 UTC, sea level pressure in mb.

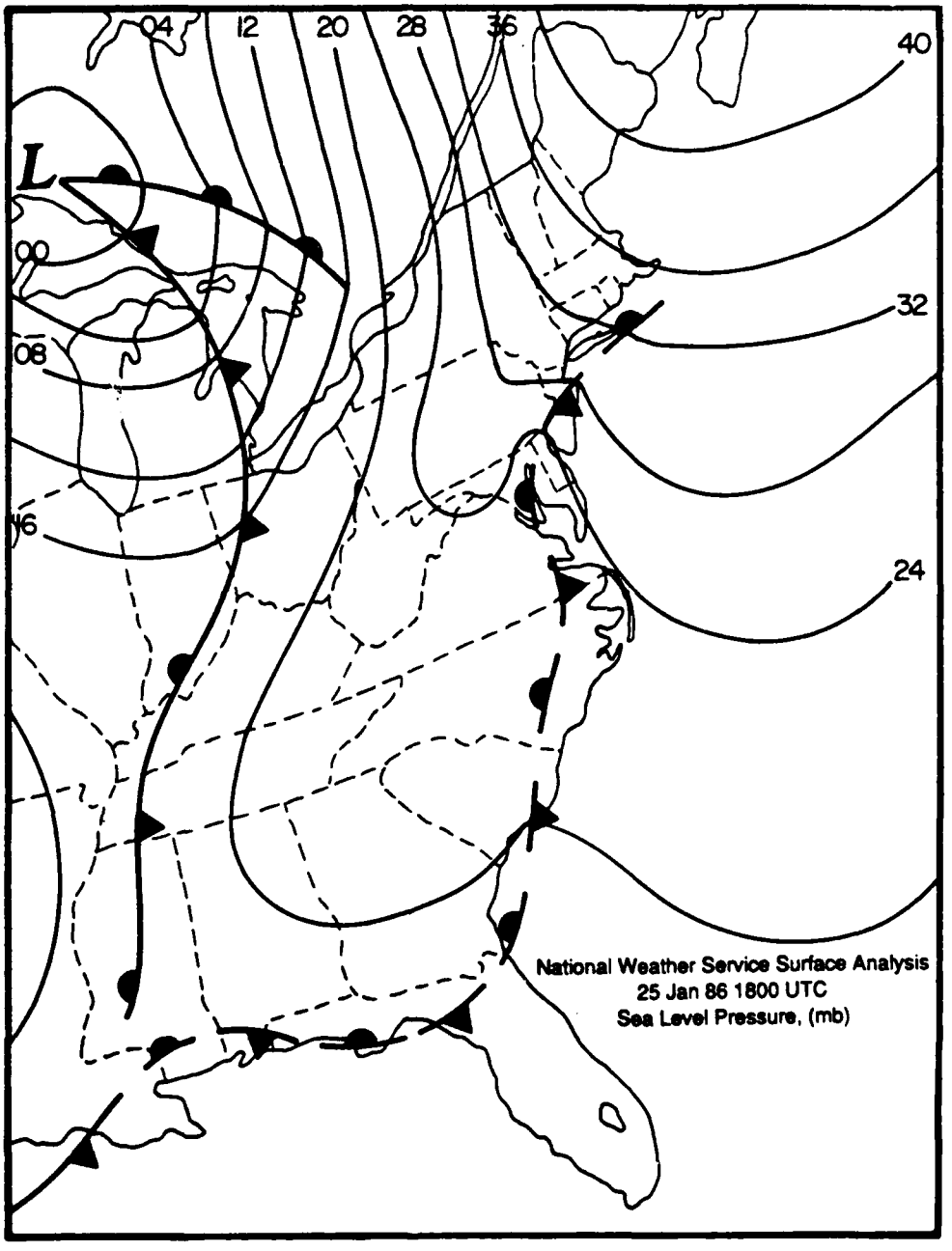

Figure 3.3b - National Weather Service Surface Analysis on 25 January 1986 for 1800 UTC, sea level pressure in mb.

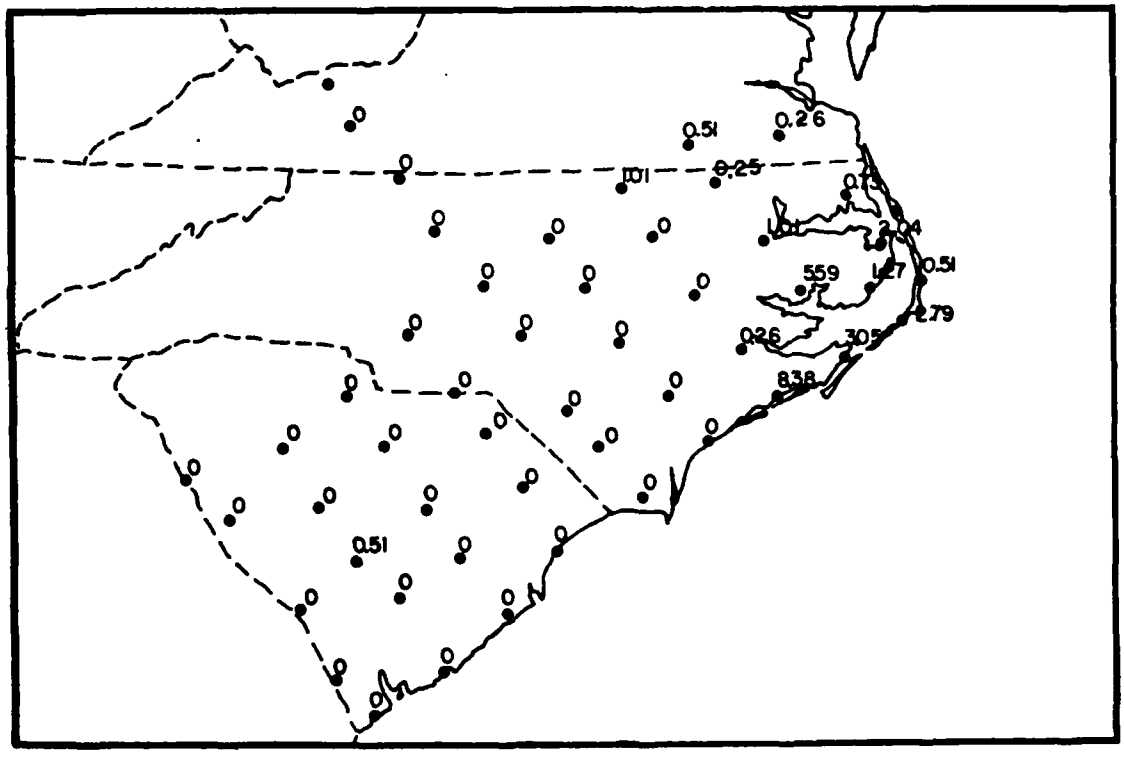

Figure 3.3c - Six hour precipitation total at PAM-II sites, measured in mm.

3.2 Mesoscale Analysis Of The Coastal Front

3.2.1 Surface Analysis

The mesoscale analyses to be shown were based on measurements from the PAM network, NWS stations, buoy, and ship hourly reports. The PAM data were not used in the pressure analysis because development of PAM pressure-correction procedure is still in progress by other investigators. Two different NWS Hatteras radar products were used: the first was a photograph of the PPI scope, which shows the area of precipitation; the other was a digitized image which better defines the intensity of the precipitation.

Early on the 25 January the average flow over the Carolinas is from the northwest. However, there is onshore flow in the vicinity of Cape Hatteras associated with a weak temperature gradient. There is also an area of convergence over the Pamlico Sound and just inland. The surface pressure analysis depicts an area of high pressure elongated along the Appalachian Mountains. This again is supportive of the cold-air damming on the east side of the mountains. The satellite picture shows overcast skies throughout the Carolinas with higher clouds over the mountains.

The coastal front becomes evident inland prior to 1200 UTC 25 January. Earlier, the front lay offshore near the zone of strong temperature gradient (between the cold water and the Gulf Stream)

and extends southwest from the southern tip of North Carolina and offshore parallel to the coast of South Carolina. The front passes PAM site 45 (located on the outer banks of North Carolina, just south of Cape Hatteras) at approximately 0800 UTC. A time series of PAM site 45 observations can be found in Figures 3.6a and 3.6b. There is a strong temperature change (3°C) and a wind shift of 60 degrees from 0700 to 0800 UTC, both of which are indicative of a frontal passage. There is a large area of convergence along eastern North Carolina, as far west as PAM station 42. No precipitation was recorded at the PAM sites, but the Hatteras radar indicates there is activity along the Outer Banks and along a north/south line 100 miles inland.

There is little change in the position or the intensity of the front until after sunrise. At 1200 UTC 25 January the surface analysis (Fig. 3.3a) depicts an inverted trough along the East Coast. There is still a cold northerly wind on the east side of the mountains. With a southeast wind off the Carolina Coast, the directional wind shear across the trough is approximately 150 degrees. The surface analysis for 1200 UTC 25 January (Fig. 3.4a) depicts the temperature gradient in eastern North Carolina, across PAM stations 42 to 48, as 6°C. The gradient, across the same distance, off the coast near Wilmington is 10°C, a much sharper difference, partly because of the discontinuity in surface temperature between the colder land mass and much warmer Gulf Stream (Fig. 3.4b). Associated with the

coastal front is some precipitation recorded at PAM sites 35, 37, and 40. In addition, the Hatteras radar shows a larger area of precipitation over the southern part of the Pamlico Sound. This is in the area of convergence, as computed by the Barnes analysis scheme, and in the vicinity of the coastal front.

By 1300 UTC 25 January, there is continued strong convergence along the front, and the thermal gradient begins to strengthen along the Virginia coast and off the southern portion of the North Carolina coast. The northern portion of the coastal front begins to move further inland, pushing westward past PAM station 50. Also, there is a small lobe of convergence further inland from the coastal front which stretches northward from the North Carolina coast northeast of Wilmington (PAM site 30 to site 37). The convergence pattern can be seen from the wind directions, wind at site 36 is east-northeast and at site 37 is northwest. Further, notice that site 36 (with an east-northeast wind) is west of the analyzed coastal front location. Again, the Hatteras radar shows an abundance of activity over eastern North Carolina. There is only one PAM site that registers frontal precipitation, site 35.

By 1400 UTC (Fig. 3.4c) an interesting circulation has developed in the area near stations 35, 36, 40, and 41 (located in the southern part of Pamlico Sound); a small divergent cyclonic feature is noticeable. In the previous hour the coastal front was positioned through this area. Now the circulation and divergence appear to be

destroying and dividing the front so that by 1400 UTC there appears to be two frontal boundaries (Fig. 3.4c), one further inland and the other east of the area of divergence and closer to the coast.

There are several different possible reasons for the development of the divergent eddy. First, the formation of the eddy can be described as a frontal wave development (Riordan, 1989). The portion of the offshore coastal front located just south of Pamlico Sound remains offshore just east of Cape Lookout, while the northern portion of the front propagates west across the sound. Thus, the coastal front becomes S shaped, folds over and forms a small cyclonic eddy. A second mechanism of eddy formation involves differential heating between the land and Pamlico Sound. The timing of the appearance of the eddy just after sunrise seems to suggest a direct thermal circulation. However, such a sea-breeze type flow would be associated with onshore wind components while the station closest to the shoreline and which undergoes the largest wind shift, namely PAM site 40, has an offshore flow. Whatever the mechanism for its development, the formation of this eddy appears to be related to the topography. However, since the scale of the eddy is too small for the PAM network to resolve, the reasons for its formation remain unknown at present.

The appearance of two "fronts" may be due to several processes: first, since the cold air trapped to the east of the mountains is a very shallow layer, it may be easily eroded from above; second, the

thinning clouds may have allowed enough solar radiation to heat the surface and destroy portions of the cold-air wedge from the surface up. We will investigate these possibilities in a later section.

After the westward "jump" of the original coastal front, the second boundary remains over Pamlico Sound and appears to be a natural feature coinciding with the Sea Surface Temperature (SST) boundary formed by the cold shelf and sound water and the adjacent warm Gulf Stream (Fig. 3.4b). For example, the water in the Pamlico Sound and along the coast is 6-8 °C and the Gulf Stream water is 20-24 °C. Note that the precipitation is associated with the secondary boundary; the four PAM sites that received precipitation are located near the coast. Further, the radar images show a much larger area of precipitation, almost completely covering the Pamlico Sound.

By 1500 UTC (Fig. 3.4d) the NWS surface analysis depicts the inverted trough just west of Pamlico Sound then extending offshore and aligned parallel to the coastline to the south. A detailed mesoscale analysis (including NWS sites, ships, and buoys) of this area shows details not previously seen. Analyses based on either temperatures or winds agree that the coastal front is, in fact, further inland across southern North Carolina. The temperature gradient is also strengthening ahead of the inland coastal front. The stronger gradient may be due to the increased solar radiation near the coast, where the sky has become scattered or clear. The second

boundary is again present over the Pamlico Sound and precipitation is still associated with this boundary. However, the absence of apparent radar activity inland may be due to the fact that any such echoes would be moving out of range of the Hatteras radar.

Over the next few hours the inland coastal front strengthens, while the boundary that is associated with the warm onshore flow over Pamlico Sound weakens. The flow along the southern North Carolina coast is onshore and there is a large area of convergence along the inland coastal front. Again, according to the Hatteras radar, the precipitation is confined almost exclusively to Pamlico Sound and is associated with the weakening frontal boundary. The only area of precipitation measured by the PAM sites is over Pamlico Sound.

By 1800 UTC the temperature gradient has become more complicated (Fig. 3.4e). West of the front the isotherms are tightly packed, as expected with a frontal system. Immediately east of the front the air temperature is constant, while further east along the coast of North Carolina, over Pamlico sound, the air is again warmer. Along the southern coast of North Carolina there is a small pocket of colder air which remains throughout the next few hours. In addition, the offshore air over the Gulf Stream is still warming. Finally, figure 3.4f depicts the digitalized GALE radar mosaic for 1800 UTC 25 January 1986. The large area of echo returns are along the coast and in the vicinity of the orphan coastal front.

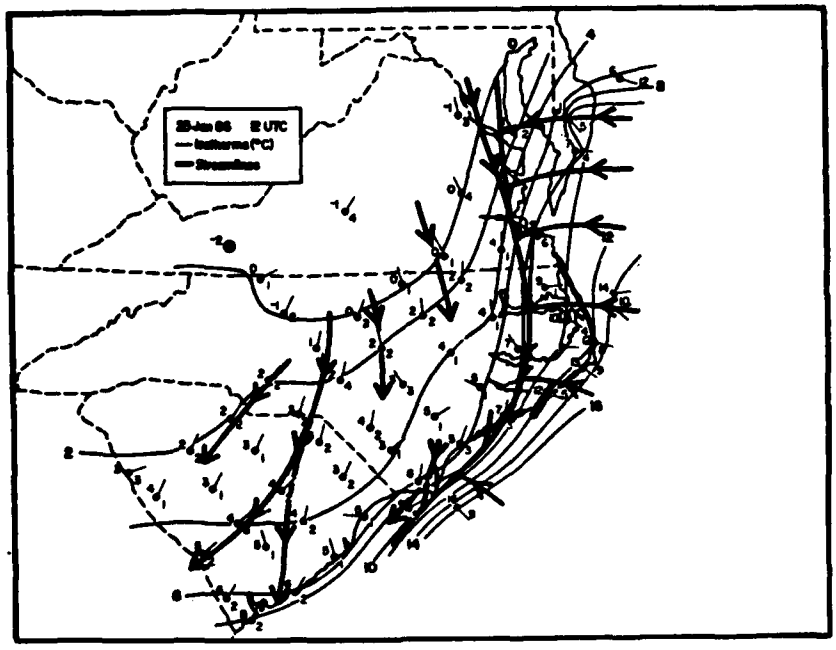

Figure 3.4a - Surface Analysis for 1200 UTC 25 January 1986. Thin lines depict isotherms every 2 degrees (C), thick lines are streamlines analyzed using winds greater than 2 m/s. Frontal boundary is denoted by the heaviest streamline. Station reports include temperature (C) and wind speed (M/S).

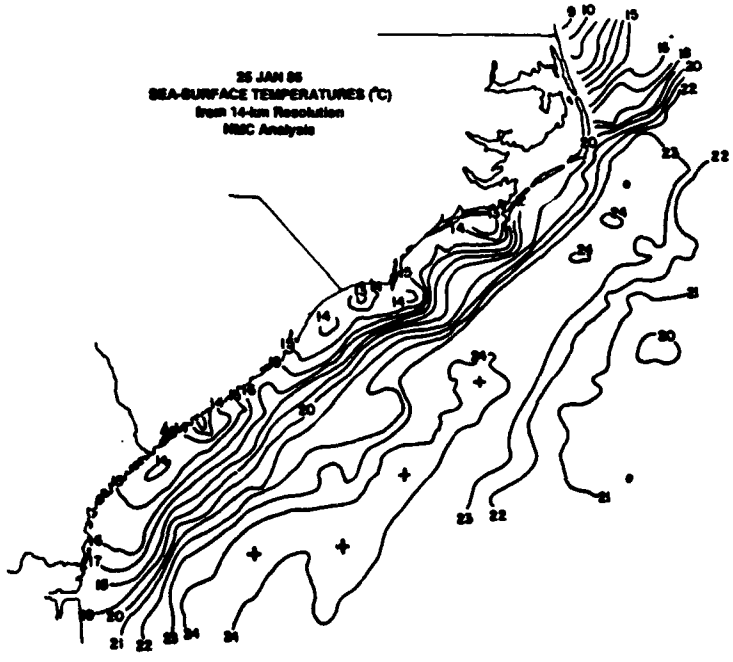

Figure 3.4b - Sea-surface temperature (C) for 25 January 86 obtained from 14km resolution analysis, derived from satellite and in-situ data.

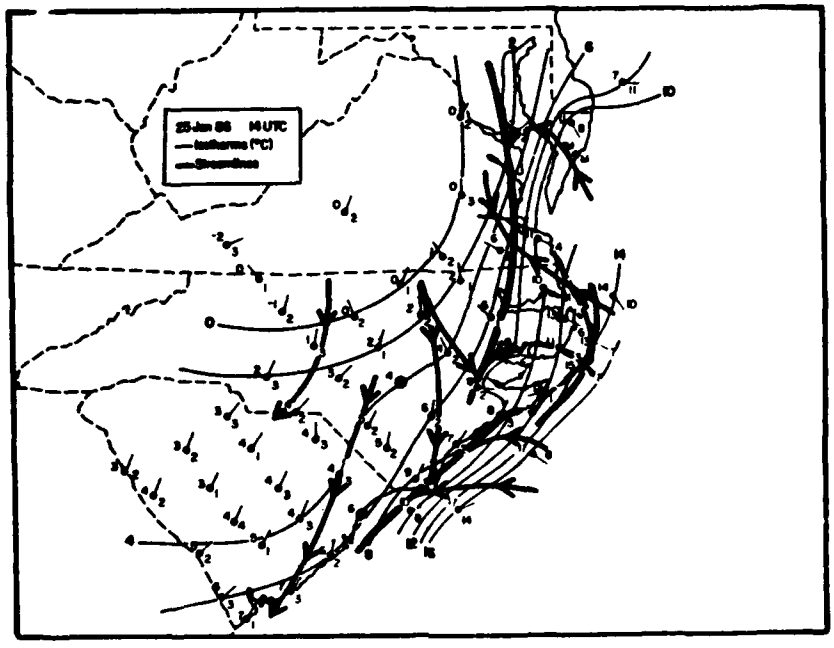

Figure 3.4c - Same as Figure 3.4a except for 1400 UTC 25 January 1986.

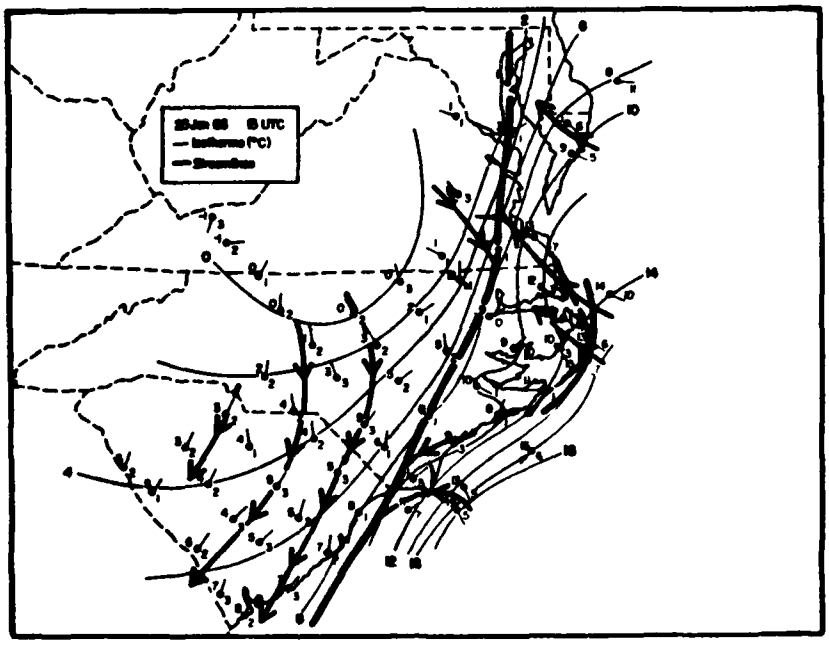

Figure 3.4d - Same as Figure 3.4a except for 1500 UTC 25 January 1986.

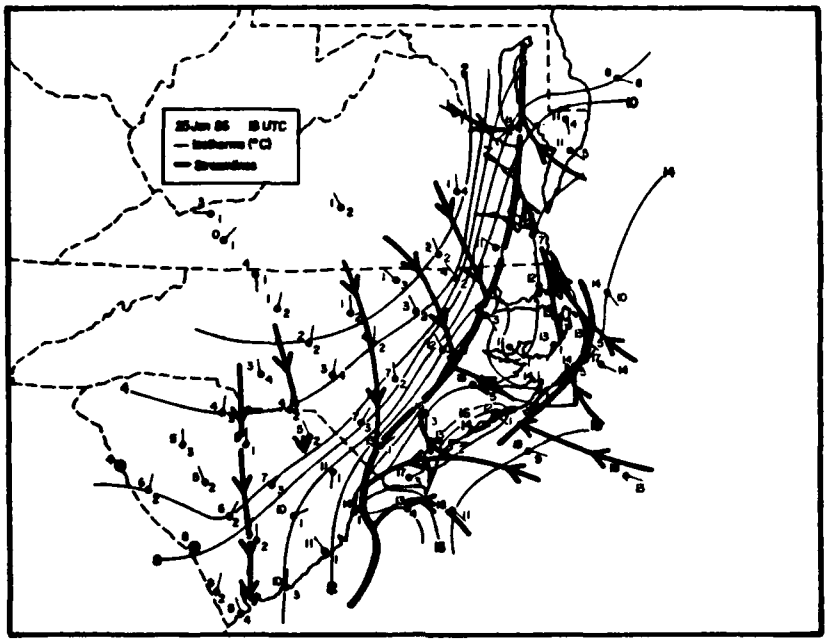

Figure 3.4e - Same as Figure 3.4a except for 1800 UTC 25 January 1986.

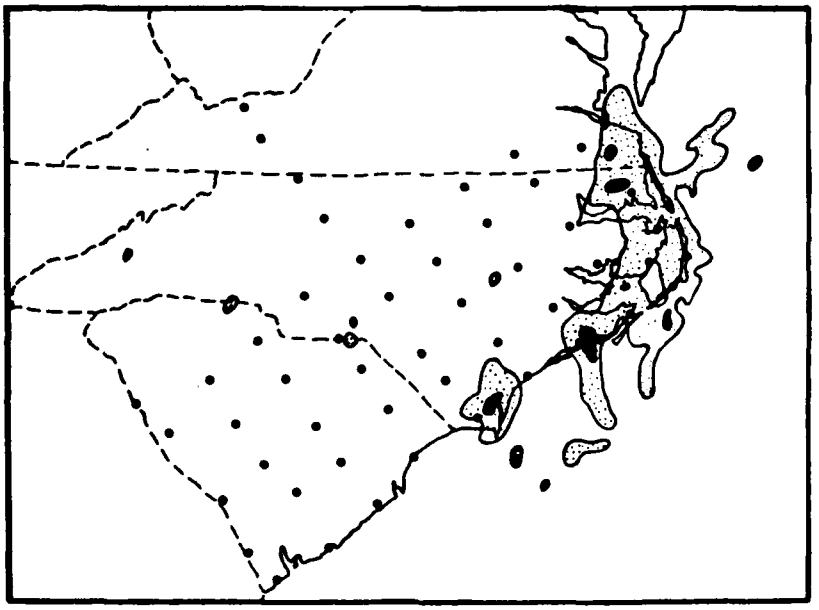

Figure 3.4f - Radar depiction for 1800 UTC 25 January 1986. The dotted areas are echo returns up to 25 dBZ, the darkened areas are returns greater than 25 dBZ.

3.2.2 Cross Section Analysis

The vertical cross sections, along a line joining Hatteras (HAT), Greenville (PGV), and Greensboro (GSO) N.C., are based on data from the 1200 UTC (Fig. 3.5a) and 1800 UTC (Fig. 3.5b) 25 January 1986 soundings. The cross section was analyzed from the surface to 800 mb. The most important part of the analysis is the lower 100 mb since the coastal front is a low-level phenomena.

The 1200 UTC cross section depicts a strong horizontal temperature gradient of 9 °C/105 km associated with the coastal front between PGV and HAT. By 1800 UTC the major part of the frontal gradient has sharpened and moved west near the surface, but has left behind a weaker eastern portion near Hatteras. The latter feature is referred to hereafter as the orphan front.

The inland front has a much sharper thermal gradient than the orphan front along the coast. But the orphan front has continuity to a much higher level, namely up to about 850 mb. Thus, the air mass along the coast is not just a cold shallow pocket of air, but a reasonably deep frontal system. It is thus a possible forcing mechanism for the scattered rainshowers observed along the coast.

The location and structure of the frontal zone can also be seen in the wind field. The 1200 UTC winds at Hatteras are from the east (90 degrees). The low-level winds over PGV are also from the east, while above the frontal boundary they are from the south. Over GSO there is a sharp veering of the wind with height marking the frontal

zone: at 960 mb the winds are from the northeast (30 degrees) and at 940 mb the winds are from the south (180 degrees). By 1800 UTC the winds over HAT have become more southeasterly (140 degrees) and become even more southerly with height. Over PGV the winds change from southeast at the surface to southerly aloft. Over GSO there again is a large vector wind shear through the front.

The water vapor distribution remains similar throughout the period. At 1200 UTC there is a tongue of moist air, extending inland from offshore, just above the frontal surface. The 1800 UTC analysis depicts more moisture moving onshore than the 1200 UTC analysis. The frontal zone along the coast and the moist air moving onshore are supportive of the observed scattered rainshowers along the coast.

In summary, the cross sections help explain why the rainshowers recorded on the 25th are generally confined to the coastal region. There is a persistent frontal boundary present along the coast which may provide a mechanism for the showers.

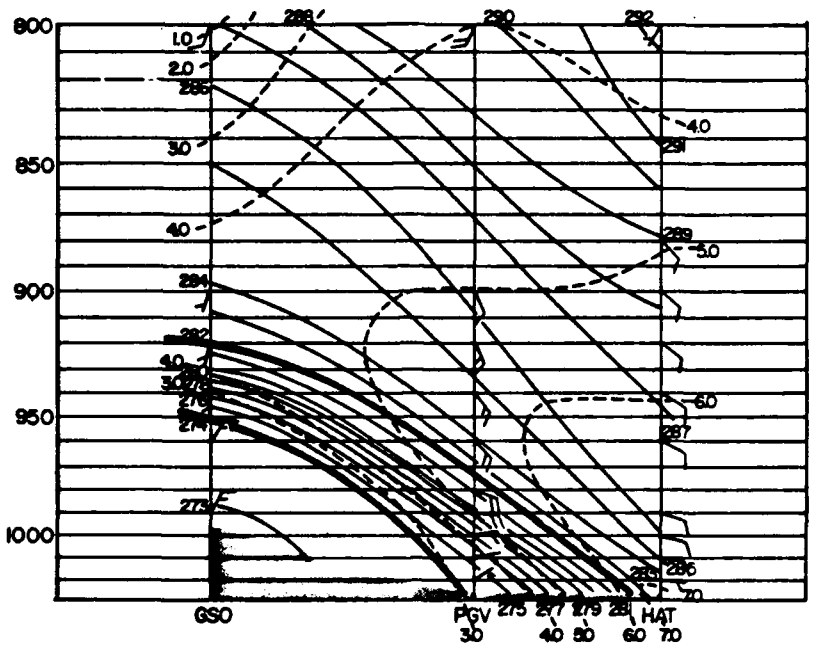

Figure 3.5a - Cross-sectional analysis from Greenville, NC (PGV) to Hatteras, NC (HAT) at 1200 UTC 25 January 1986. Solid lines depict potential temperature (K), thin dashed lines depict mixing ratio (g/kg), and wind vectors are shown with whole barbs for each 10 m/s. Frontal boundaries are highlighted by the thick lines.

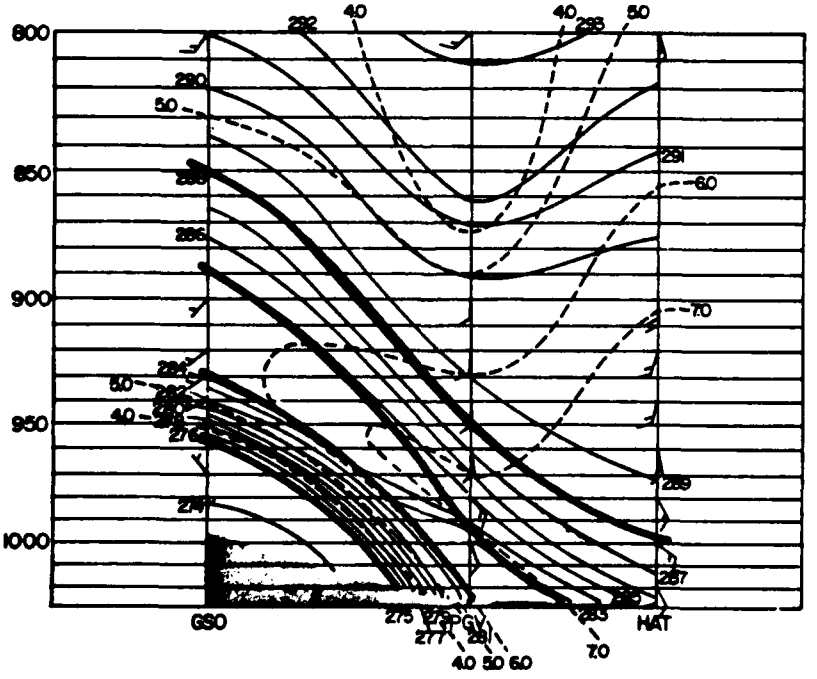

Figure 3.5b - Same as figure 3.5a except for 1800 UTC 25 January 1986.

3.2.3 Time Series at PAM Site 45

This study involves following a coastal front, so it's important to identify exactly when a frontal system passes through an area (in this case the PAM network). Following the events in time at one location quickly identifies when a frontal system passes that location. This time series utilizes PAM site 45 because it is the farthest east and will be least affected by the land mass. Frontal systems are identified by a sharp discontinuity in temperature and a simultaneous sharp change in wind direction, so these two events will be examined. Figure 3.6a and b depict the change in temperature and wind direction with time. Notice the overnight temperature (Fig. 3.6a) is around 9°C. Between 0700 UTC and 0800 UTC there is a temperature jump of three degrees. The temperature warms slowly through the rest of the day, except for a two degree jump between 1300 UTC to 1400 UTC. The second temperature increase is probably due to a short-term clearing of the clouds.

The wind direction (Fig. 3.6b) until 0700 UTC is 30 degrees. Between 0700 UTC and 0800 UTC the wind direction veers to about 90 degrees, throughout the rest of the day the wind slowly becomes more southerly. The change in wind direction clearly shows that the coastal front moves past PAM site 45 between 0700 and 0800 UTC on the 25th.

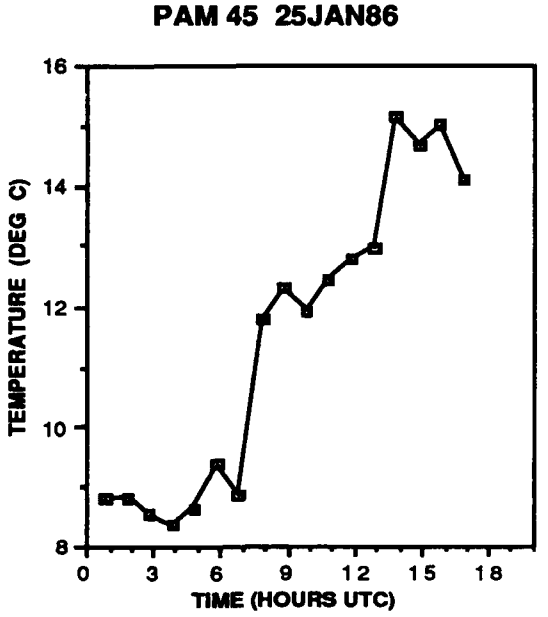

Figure 3.6a - Time series at PAM-II site 45 from 0050 UTC 25 January 1986 to 1750 UTC 25 January 1986. The temperature (C) is plotted against time.

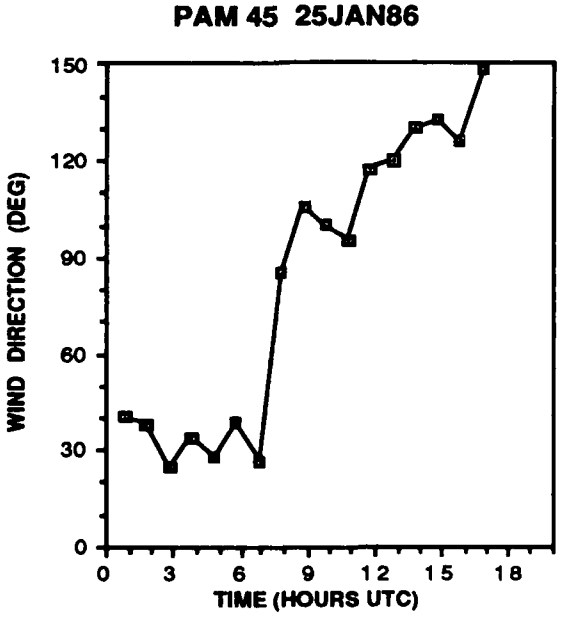

Figure 3.6b - Time series at PAM-II site 45 from 0050 UTC 25 January 1986 to 1750 UTC 25 January 1986. The wind direction (deg) is plotted against time.

3.2.4 Tower Data

Carolina Power and Light Company maintains three meteorological towers in North and South Carolina. They are located at the Shearon-Harris Nuclear Plant, North Carolina (35 ° 38.7 ' North and 78 ° 56.7 ' West), the Brunswick Nuclear Plant, North Carolina (33 ° 57.8 ' North and 78 ° 00.8 ' West), and the Robinson Nuclear Plant, South Carolina (34 ° 24.0 ' North and 80 ° 9.1 ' West). The Brunswick tower is about 100 meters high and has sensors 11 meters above the surface and near the top of the tower. The Shearon-Harris and Robinson towers are about 60 meters high and the sensors are located about 10 meters above the ground and near the top of the tower. The measurements at all sites are averaged over 15 minutes; the data that will be utilized are the solar radiation, surface temperature, difference between the upper temperature and the lower temperature, and the lower wind direction and speed.

The tower data can provide information on both sides of the coastal front. These data may help to show whether there is sufficient surface heating to destroy the original coastal front and aid in the formation of the two coastal fronts. Throughout the morning and afternoon the Brunswick Tower is located east of the front, while the Shearon-Harris Tower is located well inland of the front. First, the data from the Brunswick Tower will be examined and will be compared to PAM site 21, located west of the tower,

along the coast. Since PAM site 21 is west of the tower, the front should pass PAM 21 after first passing the tower.

The Brunswick Tower data is illustrated in figures 3.7a-d and the PAM 21 data is illustrated in figure 3.7e-h. Measurements at the PAM site (Fig. 3.7 e and f) indicate the frontal passage sometime near 1500 UTC. Examination of the 5 minute data (Fig. 3.7 g and h), suggests two frontal passages: the first occurring on 1515 UTC when there is a wind shift of 20 degrees and a jump in temperature of almost 2 degrees and the second associated with a 30 degree wind shift and a drop in temperature of about 1° C between 1615 and 1630 UTC. The drop in temperature associated with the second frontal passage is probably due to some light rain or drizzle.

If the front had previously moved west past the Brunswick Tower, it was very weak and difficult to detect. One way to test for a frontal passage is to compare the temperature difference between the base and the top of the tower to the temperature gradient in the frontal layer. As the warm front moves past the tower, the upper temperature should become warmer than the base temperature. The upper air sounding from Myrtle Beach at 1700 UTC has a maximum vertical temperature gradient in the frontal layer of 0.94 °C per 10 mb, which is roughly equal to 0.94 °C per 100 meters (the height of the tower). However, figure 3.7c depicts negative temperature differences at the tower. At no time is the temperature warmer at the top of the tower. The temperature difference is smallest around

1400 UTC perhaps indicative of a very weak front. This can also be seen in figure 3.7b. However, the Brunswick solar radiation (Fig. 3.7a) also reaches a relative maximum around 1400 UTC. Thus, the base of the tower could be warming more rapidly than the top of the tower because of solar heating.

The temperature change at the Shearon-Harris Tower is much less dramatic since the tower is located well inland and to the west of the coastal front. The base of the tower has a temperature range of only one to three degrees (Fig. 3.7i). One of the reasons for the lower temperatures is that the sky overhead remains overcast throughout the day. The corresponding solar radiation (Fig. 3.7j) measured at Shearon-Harris is considerably less and more erratic then that measured at the Brunswick tower. The maximum amount of solar radiation occurs at 1630 UTC a time corresponding to the maximum temperature difference between the top and the base of the tower (Fig. 3.7k). The amount of solar radiation steadily increases from 1300 UTC until 1515 UTC and the corresponding surface temperature and the temperature difference increase proportionally. Later in the day, as the solar radiation becomes more erratic, the temperature difference between the base and the top of the tower also becomes erratic.

The presence of superadiabatic lapse rates near the base of the tower are evidence that convective eddies may be mixing the front. Examination of the Brunswick data shows there is a superadiabatic

lapse rate in the tower layer at 1315 UTC, 1515 UTC, and between 1615 UTC and 1645 UTC. These times occur near local maxima of the solar radiation. The rest of the day the lapse rate is less then 1 degree per 100 meters and the atmosphere is probably more stable. In addition, both the measurements of the temperature difference at Shearon-Harris (Fig. 3.7k) show the lapse rate is superadiabatic throughout the day. The solar forcing is causing mixing in the lower levels throughout the entire day even on the cold side of the front.

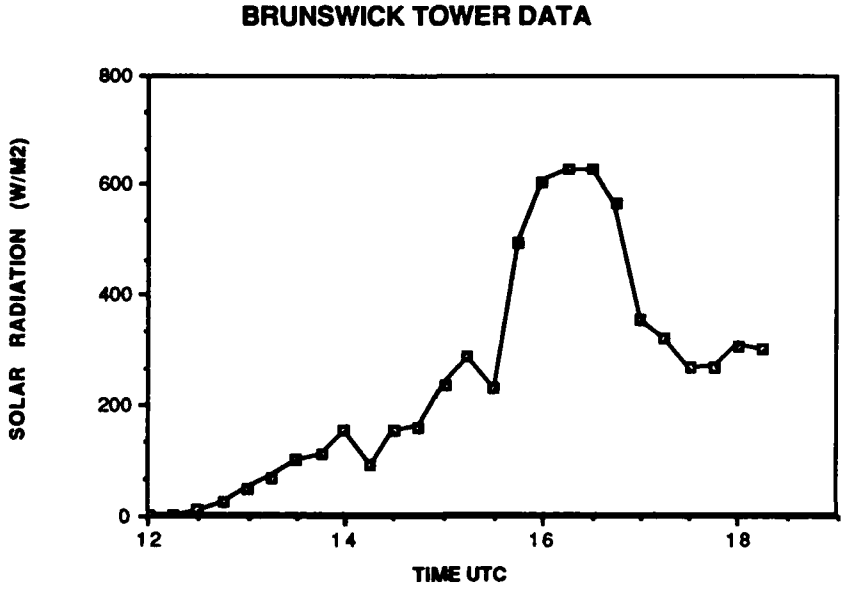

Figure 3.7a - Brunswick Tower (CP&L) data from 1200 UTC to 1800 UTC on 25 January 1986. Plot of solar radiation (W/m^2) versus time.

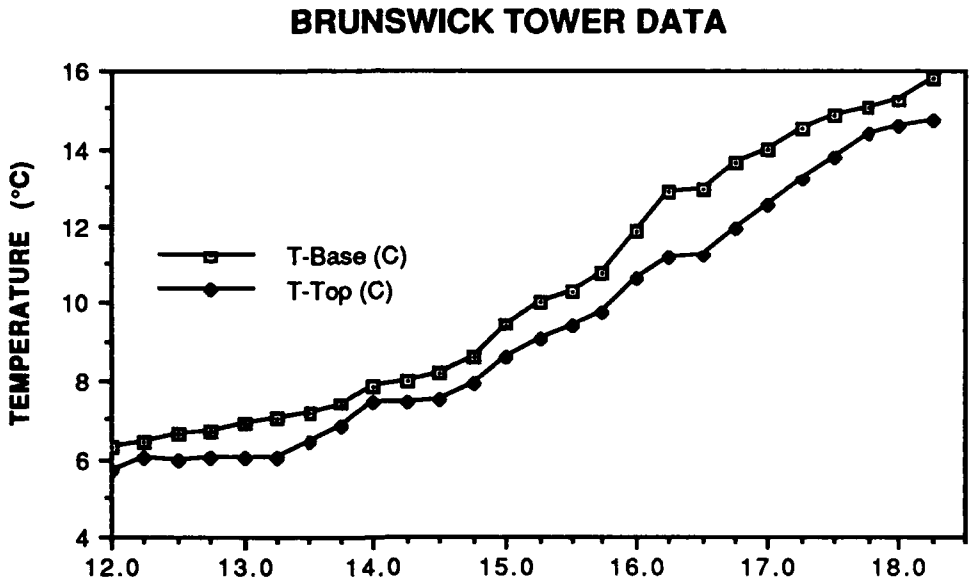

Figure 3.7b - Brunswick Tower (CP&L) data from 1200 UTC to 1800 UTC on 25 January 1986. Plot of temperature (C) versus time.

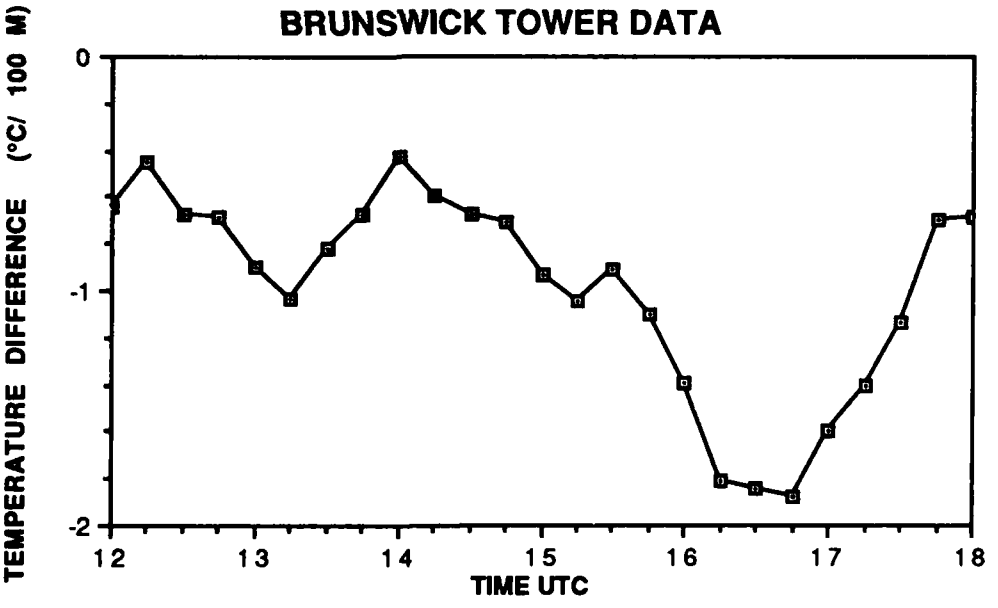

Figure 3.7c - Brunswick Tower (CP&L) data from 1200 UTC to 1800 UTC on 25 January 1986. Plot of temperature difference between the base and the top of the tower versus time.

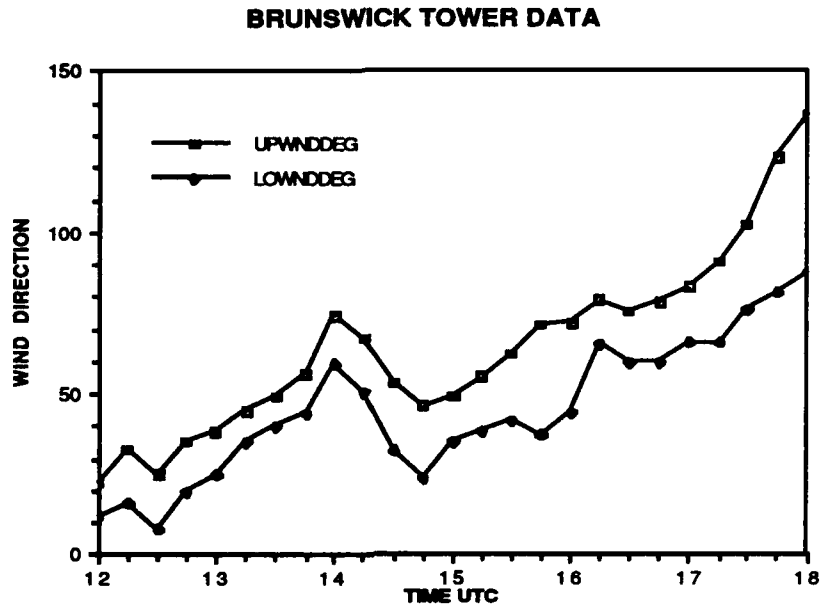

Figure 3.7d - Brunswick Tower (CP&L) data from 1200 UTC to 1800 UTC on 25 January 1986. Plot of wind direction (deg) versus time.

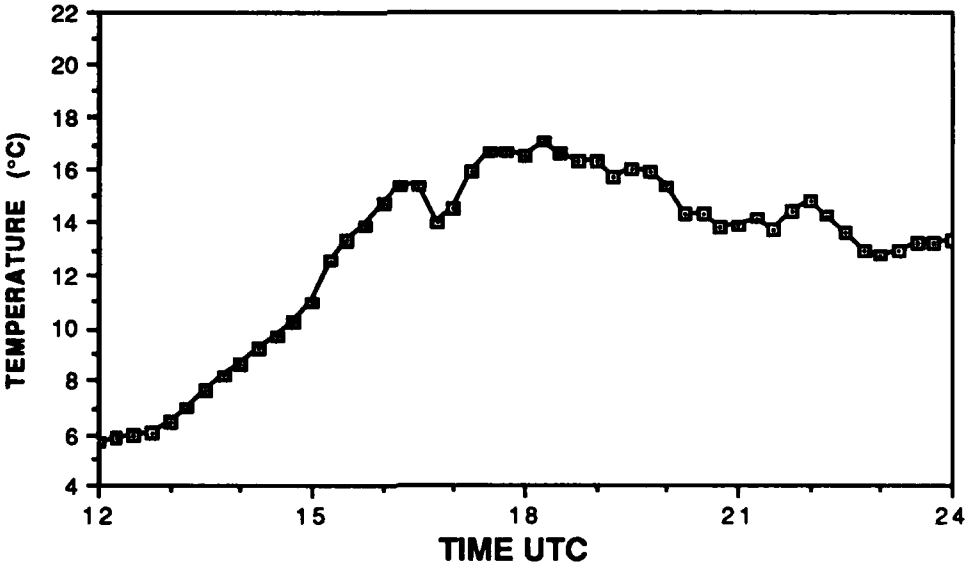

Figure 3.7e - PAM-II site 21 data from 1200 UTC 25 January 1986 to 0000 UTC 26 January 1986. Plot of temperature (C) versus time.

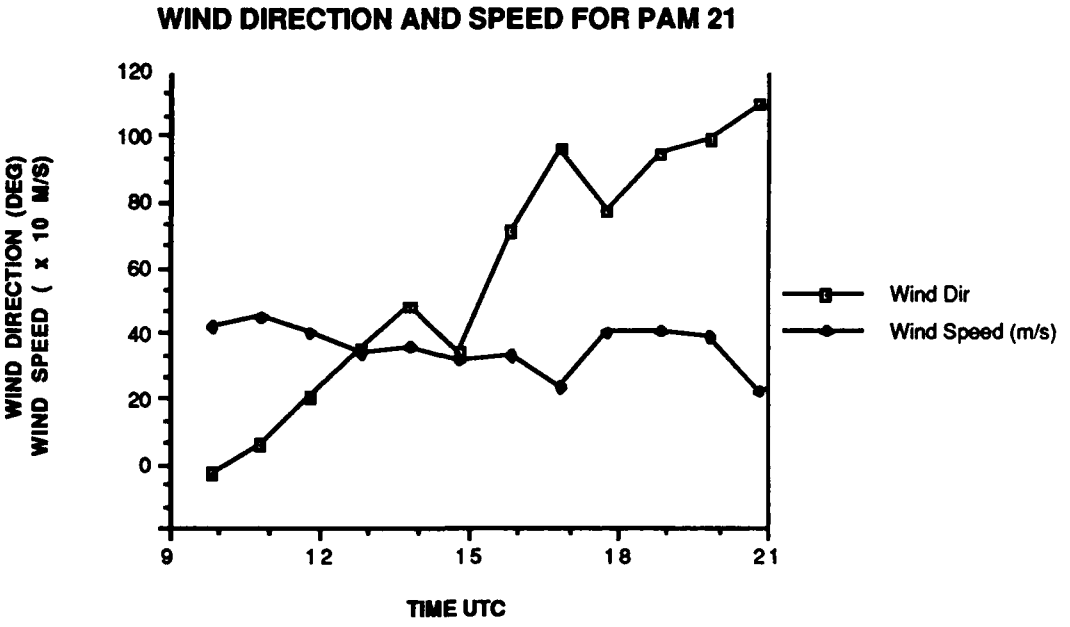

Figure 3.7f - Plot of wind direction (deg) and wind speed (m/s) versus time for PAM-II site 21 from 0950 UTC to 2050 UTC 25 January 1986.

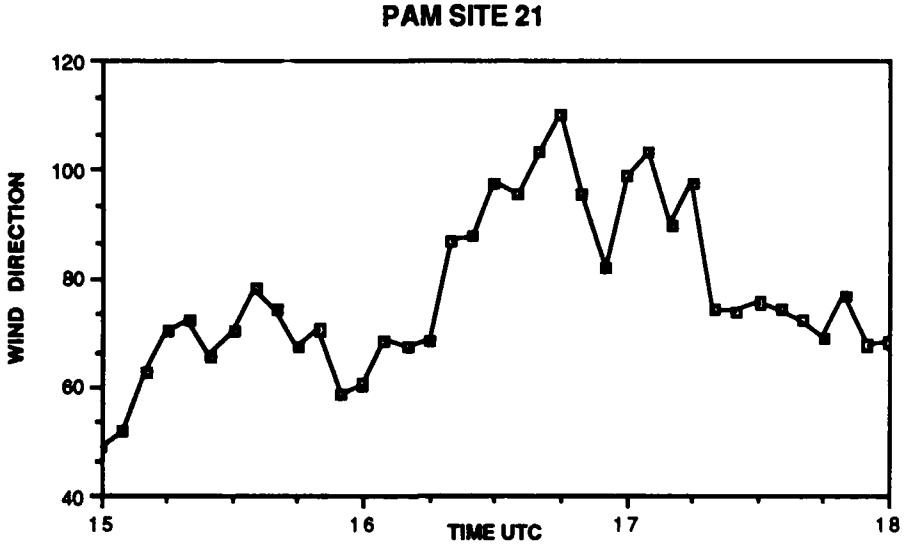

Figure 3.7g - Plot of wind direction (deg) versus time for PAM-II site 21 from 1500 UTC to 1800 UTC 25 January 1986. Wind direction is plotted every 5-minutes.

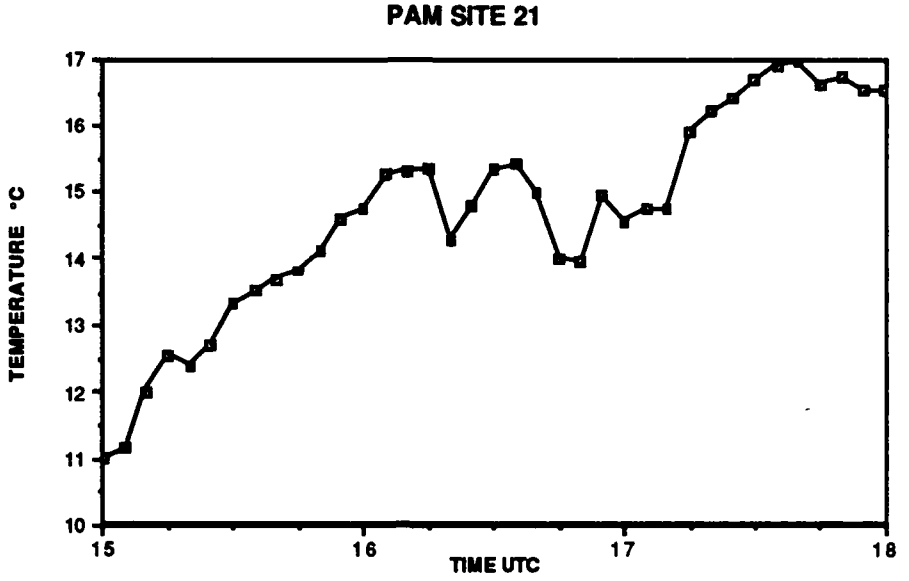

Figure 3.7h - Plot of temperature versus time for PAM-II site 21 from 1500 UTC to 1800 UTC 25 January 1986. Temperature is plotted every 5-minutes.

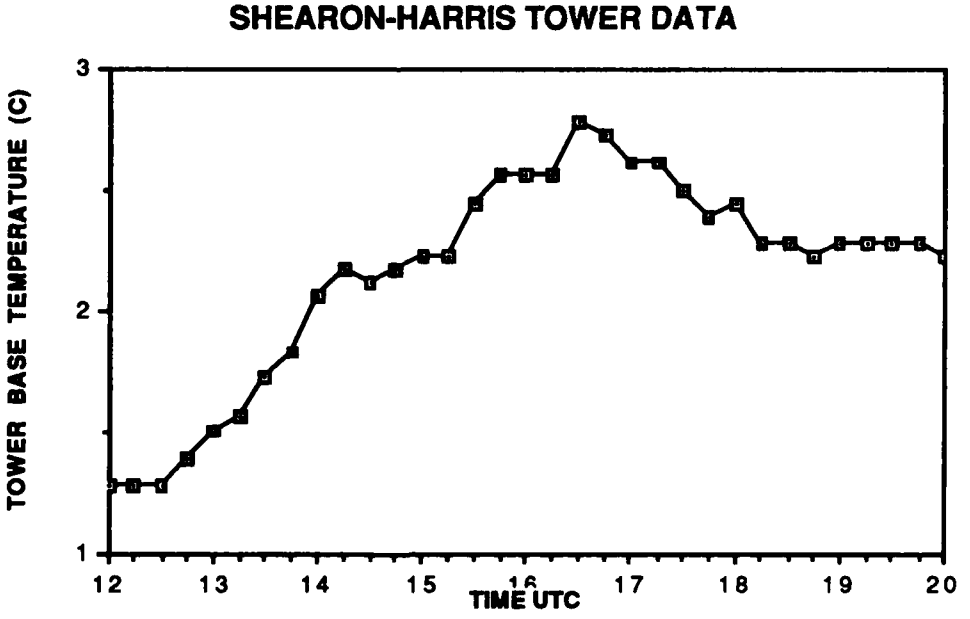

Figure 3.7i - Shearon-Harris Tower (CP&L) data from 1200 UTC to 2000 UTC on 25 January 1986. Plot of temperature at the base of the tower versus time.

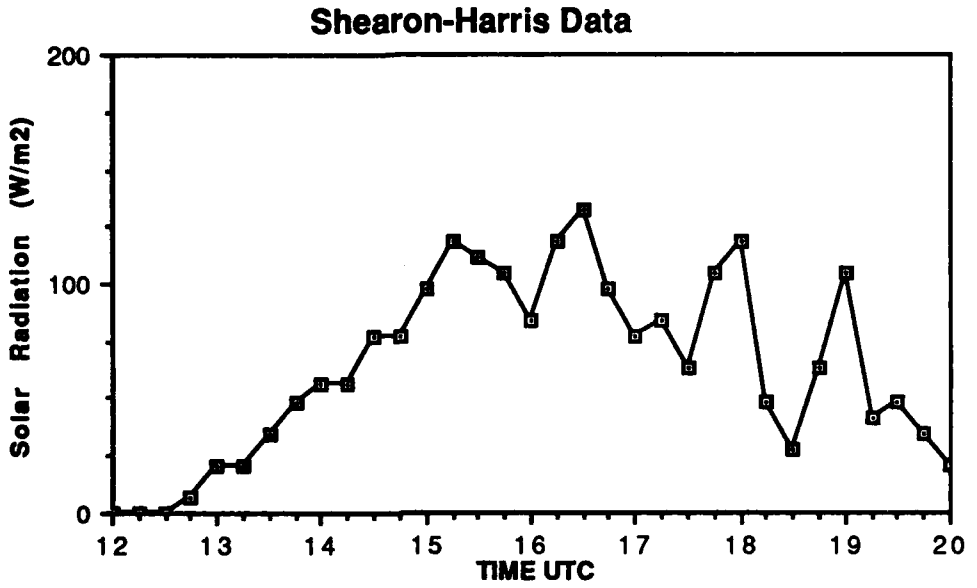

Figure 3.7j - Shearon-Harris Tower (CP&L) data from 1200 UTC to 2000 UTC on 25 January 1986. Plot of solar radiation (W/m^2) versus time.

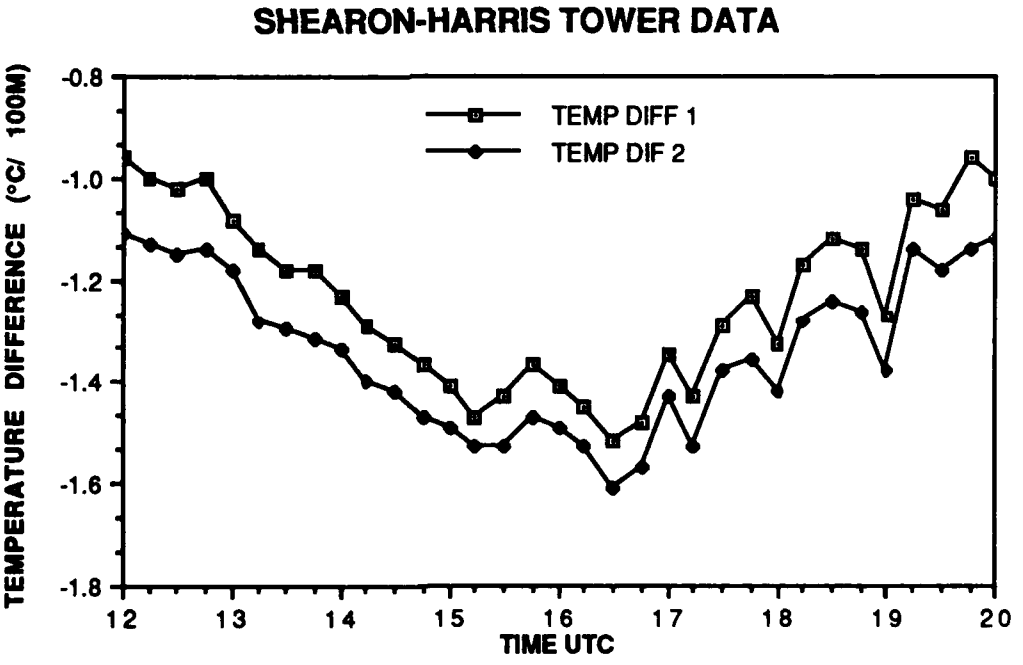

Figure 3.7k - Shearon-Harris Tower (CP&L) data from 1200 UTC to 2000 UTC on 25 January 1986. Plot of temperature difference between the base and the top of the tower versus time.

3.2.5 Turbulent Mixing (Richardson Number)

The coastal front may erode vertically and jump inland because of turbulent mixing. One way to test whether the coastal front is being mixed is by the calculation of bulk Richardson numbers (Ri), where

$$Ri = \frac{g\left(\Delta\theta_v\right)\Delta Z}{\theta_v\left(\Delta u^2 + \Delta v^2\right)}.$$

In the above equation the g is gravity, the θ_V is the virtual potential temperature, ΔZ is the thickness of the layer, Δu is the wind speed component in the x direction, and Δy is the wind speed component in the y direction. The Richardson number can be considered to represent a ratio of buoyancy to vertical shear forcing and thus is a measure of stability within a vertical layer. The value considered to be the minimum for the onset of shear instability is Ri=0.25. If turbulence is already present, Ri can be as high as 1. So, if Ri is less than 0.25, there is shear instability and there is is likely to be turbulent mixing near that level (Nieuwstadt and von Dop, 1982). The intensity of turbulent mixing at the lower frontal boundary in some sense measures the rate at which the front is being destroyed from below.

The Richardson numbers were calculated using 10-second balloon data available every 3 hours. Since the Richardson numbers are very

sensitive to small changes in shear, only the general trend can be examined. To remove some of the variability of the data, the measurements were averaged over 30-second time periods, thus utilizing four data points spanning a layer of about 120 m in depth. Also, if the wind speed differences between successive 10-second points exceeded 2.5 m/s, the point was considered to be erroneous and the GALE Data Processing Center interpolated the winds. Less than 10% of the wind readings used were interpolated. Since the calculation of the bulk Richardson number requires differencing over two levels, the data were then smoothed over 40-second periods. However, the results were so erratic that the interval was increased to 50-second periods, which utilized six data points. Finally, all locations used in the calculation were west of the coastal front so the Richardson-number profiles would characterize both the surface cold wedge and the warm air aloft.

The first location chosen was Greenville (PGV) at 0500 UTC (Fig. 3.8a). This station is located just west of the frontal system, with an inversion base at 1000 mb (approximately 200 meters). This can be seen in the PGV sounding (Fig. 3.8b). There is another temperature inversion based at 960 mb (approximately 500 meters). The Richardson numbers near the surface show the surface layer to be unstable since the Ri number is less then 0.25. Just above this boundary, there is a layer of stable air. In the second temperature inversion, the Richardson number is much higher which again

indicates more stable air. However, near the lower boundaries mixing is probably occurring as indicated by the low Richardson numbers.

Next, Greenville at 1100 UTC was examined and shown in figure 3.8c. At this time the front is closer to the station so the the cold air wedge is much shallower; the lower edge of the frontal boundary with the strong thermal gradient is based at only about 100 meters and the upper boundary is about 500 meters above the ground. The PGV sounding for 1200 UTC is shown in figure 3.8d. From figure 3.8c one can see a bell shaped curve of Ri numbers through the transition zone. Both the frontal boundaries (100 meters and near 500 meters) have a low Richardson number indicating probable mixing.

The next station examined was Fayetteville (FAY) at 1100 UTC. This station is further west than Greenville so the warm front is slightly higher. The frontal inversion has a lower boundary at about 300 meters and a strong thermal gradient associated with it. The upper boundary of the frontal zone is approximately at the 950 meter level. The results shown in figure 3.8e are quite erratic. There is a small drop in stability near the lower boundary between the air masses, but values remain above 0.25. There is little hint of mixing near the upper frontal boundary.

In summary, the Richardson numbers at PGV for 0500 UTC indicate mixing near the surface; the Richardson numbers at PGV for 1100 UTC indicate mixing between both frontal boundaries; the

Richardson number at FAY for 1100 UTC only hints of mixing near the upper boundary. So, there appears to be mixing at the frontal boundaries which causes the surface front to move westward.

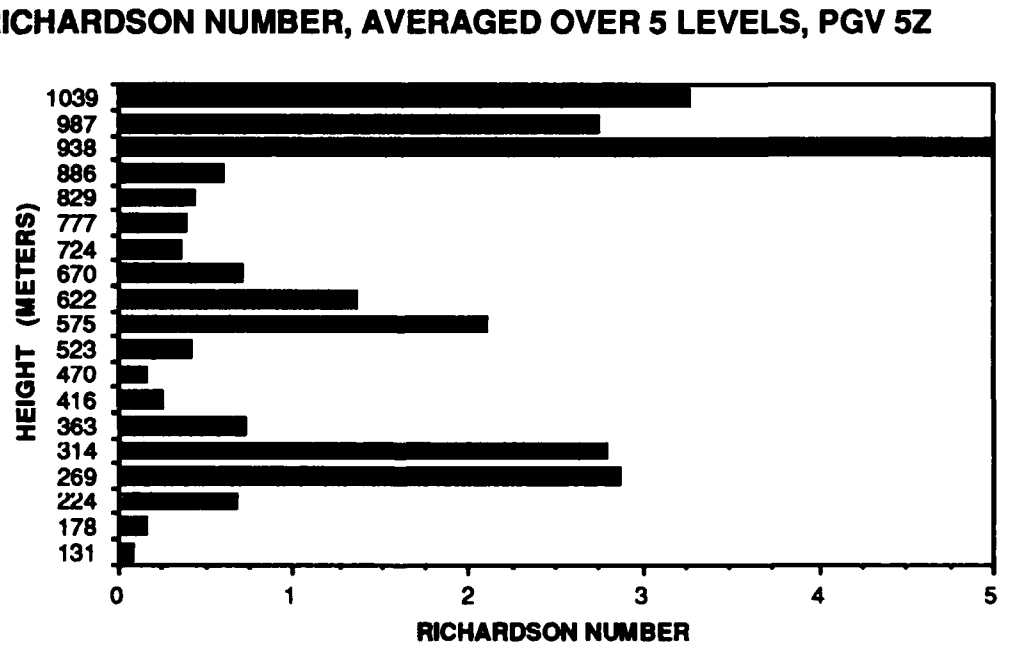

Figure 3.8a - Richardson number calculated over five levels at Greenville, NC at 0500 UTC. The Richardson numbers are plotted against different levels. The division between the cold lower layer and the warm upper layer is at approximately 200/500 meters.

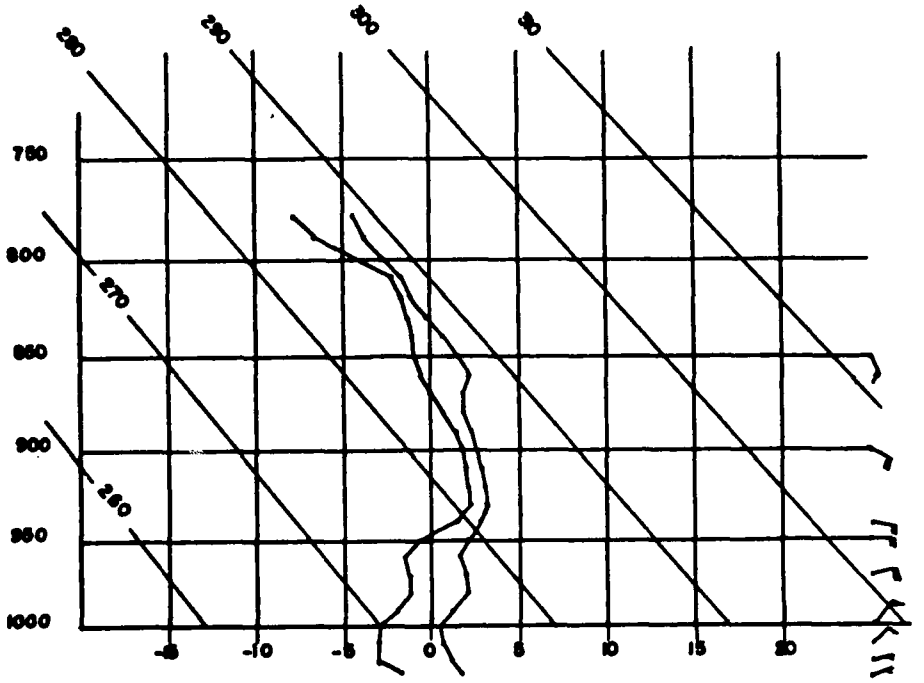

Figure 3.8b - PGV sounding at 0600 UTC

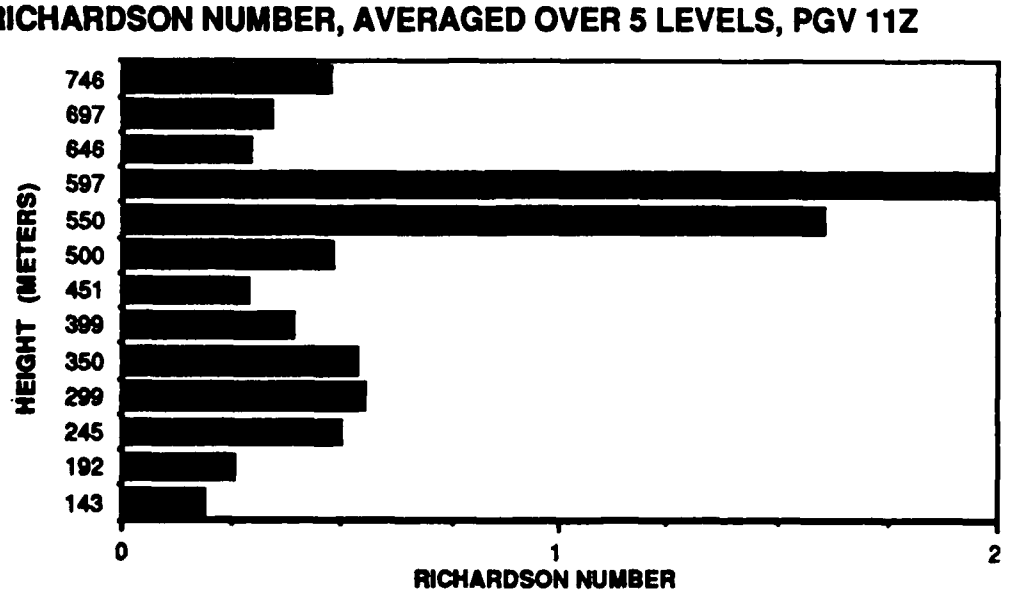

Figure 3.8c - Richardson number calculated over five levels at Greenville, NC at 1100 UTC. The Richardson numbers are plotted against different levels. The division between the cold lower layer and the warm upper layer is at approximately 100 meters.

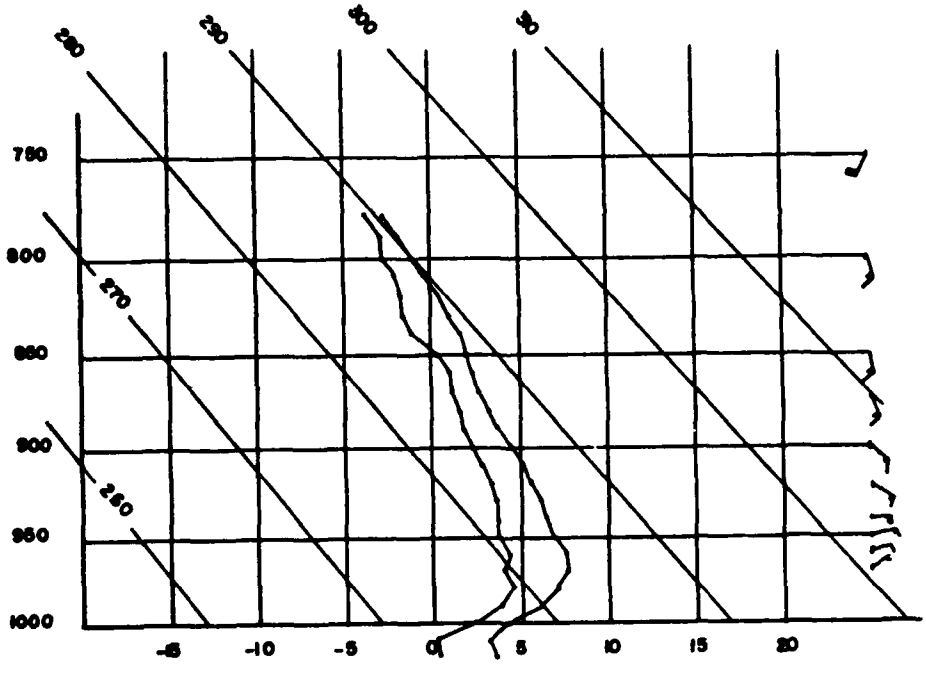

Figure 3.8d - PGV sounding for 1200 UTC

RICHARDSON NUMBER, AVERAGED OVER 5 LEVELS, FAY 11Z

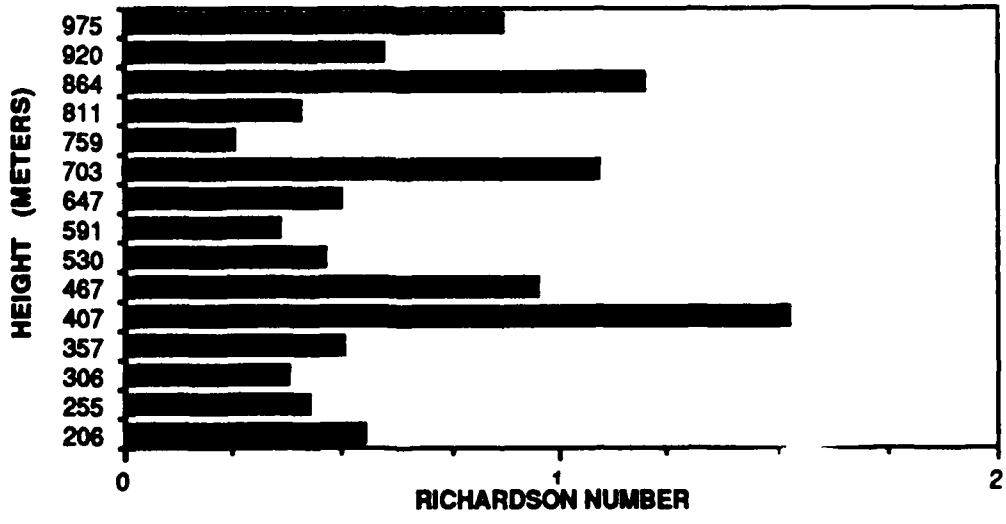

Figure 3.8e - Richardson number calculated over five levels at Fayetteville, NC at 1100 UTC. The Richardson numbers are plotted against different levels. The division between the cold lower layer and the warm upper layer is at approximately 270 meters.

4. FRONTOGENETIC PROCESS: THEORY AND EVALUATION

4.1 Frontogenesis

The intensity of two-dimensional frontogenesis, F_2, is defined as the individual rate of increase of the gradient of a scalar property S which has a continuous distribution in the horizontal plane (x,y), (Palmen and Newton, 1969, Petterssen, 1956, and Miller, 1948). That is:

$$F_2 = \frac{d}{dt}\left|\nabla_2 S\right|,$$

where $|\nabla_2 S|$ is the absolute magnitude of the X,Y gradient of S and d/dt is the time rate of change following the horizontal motion. A line along which F_2 is positive and has a maximum is called a line of frontogenesis. In addition, the line of frontogenesis must be a substantial line (Petterssen, 1956).

For the frontogenesis calculations in this research, the scalar quantity S is the potential temperature, θ. In this study the frontogenetic calculations are for near the surface, so the vertical velocity is assumed to be zero. The establishment of a front will depend on the intensity (F_2) and the duration of the process. Also, if

F_2 or any contributing process is negative or positive, it is said to be frontolytic or frontogenetic, respectively.

To examine the individual effects of confluence, shear, and advection on the intensity of the frontogenesis, the above equation is multiplied by the unit vector N_θ and d/dt is expanded. This allows for the frontogenetic calculations in the X,Y coordinate system as opposed to along and normal to the front. Thus we can write

$$F_2 = \frac{d\left|\nabla_2\theta\right|}{dt} = N_\theta \cdot \left(\frac{d}{dt}\nabla_2\theta\right) ,$$

where $N_\theta = \dfrac{\nabla_2\theta}{\left|\nabla_2\theta\right|}$.

Expanding the right-hand side of the equation yields,

$$F_2 = N_\theta \cdot \nabla_2\left(\frac{d\theta}{dt}\right) - N_\theta \cdot \left(\frac{\partial\theta}{\partial x}\nabla_2 u + \frac{\partial\theta}{\partial y}\nabla_2 v\right), \qquad (1)$$

We can also write:

$$N_\theta \cdot \frac{d(\nabla_2\theta)}{dt} = N_\theta \cdot \left[\frac{\partial(\nabla_2\theta)}{\partial t} + \tilde{V}\cdot\nabla\left(\nabla_2\theta\right)\right]. \qquad (2)$$

Equating (1) and (2), and solving for the local time-derivative, we obtain the local (Eulerian) frontogenesis:

$$\frac{\partial\left|\nabla_2\theta\right|}{\partial t} = N_\theta \cdot \left[- \tilde{V} \cdot \nabla_h\left(\nabla_2\theta\right) + \nabla_2 \frac{d\theta}{dt} - \frac{\partial\theta}{\partial x}\nabla_2 u - \frac{\partial\theta}{\partial y}\nabla_2 v \right]. \qquad (3)$$

Neglecting the diabatic effect, the local frontogenesis becomes:

$$\frac{\partial\left|\nabla_2\theta\right|}{\partial t} = N_\theta \cdot \left[- \tilde{V} \cdot \nabla_h\left(\nabla_2\theta\right) - \frac{\partial\theta}{\partial x}\nabla_2 u - \frac{\partial\theta}{\partial y}\nabla_2 v \right].$$

Using the notation $F_2 = ii\ F_x + ij\ F_y$ and $\nabla = ii\ (\partial/\partial x) + ij\ (\partial/\partial y)$, the local frontogenesis can be written:

$$\frac{\partial\left|\nabla\theta\right|}{\partial t} = -\frac{\nabla\theta}{\left|\nabla\theta\right|} \cdot \left[ii \left(u\frac{\partial^2\theta}{\partial x^2} + v\frac{\partial^2\theta}{\partial y\,\partial x} + \frac{\partial u}{\partial x}\frac{\partial\theta}{\partial x} + \frac{\partial v}{\partial x}\frac{\partial\theta}{\partial y} \right) \right.$$

advection confluence shear

$$\left. + ij \left(u\frac{\partial^2\theta}{\partial x\,\partial y} + v\frac{\partial^2\theta}{\partial y^2} + \frac{\partial u}{\partial y}\frac{\partial\theta}{\partial x} + \frac{\partial v}{\partial y}\frac{\partial\theta}{\partial y} \right) \right].$$

advection shear confluence

Combining similar terms from above, the individual contributions to total frontogenesis are:

$$\text{Advection} = -\frac{\partial\theta}{\partial x}\frac{1}{\left|\nabla\theta\right|}\left(u\frac{\partial^2\theta}{\partial x^2} + v\frac{\partial^2\theta}{\partial y\,\partial x} \right) - \frac{\partial\theta}{\partial y}\frac{1}{\left|\nabla\theta\right|}\left(u\frac{\partial^2\theta}{\partial x\,\partial y} + v\frac{\partial^2\theta}{\partial y^2} \right)$$

$$\text{Confluence} = -\frac{\partial\theta}{\partial x}\frac{1}{|\nabla\theta|}\frac{\partial u}{\partial x}\frac{\partial\theta}{\partial x} - \frac{\partial\theta}{\partial y}\frac{1}{|\nabla\theta|}\frac{\partial v}{\partial y}\frac{\partial\theta}{\partial y}$$

$$\text{Shear} = -\frac{\partial\theta}{\partial x}\frac{1}{|\nabla\theta|}\frac{\partial v}{\partial x}\frac{\partial\theta}{\partial y} - \frac{\partial\theta}{\partial y}\frac{1}{|\nabla\theta|}\frac{\partial u}{\partial y}\frac{\partial\theta}{\partial x}.$$

The ***total adiabatic frontogenesis*** (parcel following or Lagrangian) can be expressed as the sum of the confluence and shear terms :

$$F_2 = \frac{d|\nabla\theta|}{dt} = \text{Confluence} + \text{Shear}.$$

Finally, since $d\theta/dt = \partial\theta/\partial t + V\cdot\nabla_2\theta$, the diabatic term in (3) can be written:

$$N_\theta \cdot \nabla_2\left(\frac{d\theta}{dt}\right) = \frac{\nabla\theta}{|\nabla\theta|}\cdot\left[\vec{i}\frac{\partial^2\theta}{\partial x\partial t} + \vec{j}\frac{\partial^2\theta}{\partial y\partial t}\right] + \text{Advection} + \text{Confluence} + \text{Shear}.$$

4.1.1 Frontogenesis Results

The National Weather Service and PAM II data were combined and interpolated to grid points by the Barnes scheme as described earlier. Then the frontogenesis terms were computed from the surface temperature and winds using standard second-order centered differences. Gridded fields of temperature, temperature

gradient, and the separate frontogenetic processes and their combined effects were analyzed at one hour intervals. Of interest is the relative magnitudes of the confluence, shearing, and advection terms to the total and local frontogenesis.

The results for local frontogenesis for the period 1200 UTC to 1800 UTC are shown in figures 4.1a, 4.1e, 4.1f, 4.1j, and 4.1k. These maps depict the local frontogenesis calculations with negative regions represented by hatched areas and values greater than 1°K/100km/hour are shaded gray. The hand-analyzed frontal position is shown as well as the 50-station PAM-II network, surrounding hourly observations, and the grid mesh.

There are several common characteristics on all the maps. First, the local frontogenesis is weakly negative (frontolytic) over the western portion of the analysis. Next, there is an area of positive frontogenesis mainly due to convergence along the coast near Cape Hatteras after 1300 UTC. Finally, there is consistently another area of frontolysis over central South Carolina.

Local frontogenesis is examined at 1200 UTC 25 January 1986 (figure 4.1a). There is a local frontogenetic maximum (1.4°K/100km/hr) along the inland front throughout it's extent, and increasing to a maximum of about 3°K/100km/hr offshore. Upon examination of the shear (Fig. 4.1b), confluence (Fig. 4.1c), and advection maps (Fig. 4.1d), it becomes apparent that confluence is the dominant factor in frontogenesis in eastern North Carolina. The shear and advection have little effect on the overland local

frontogenesis. Both the shear and confluence terms are stronger along the offshore front; the shear maximum is nearly 2°K/100km/hr and the confluence term is 1.3°K/100km/hr.

By 1300 UTC (Fig. 4.1e) there is little change in position of the frontal boundary and the local frontogenesis maximum is still 1.4°K/100km/hr. The confluence along the front over eastern North Carolina is again the dominant term of frontogenesis, with a maximum of 1.3°K/100km/hr. The confluence and shear add nearly 2°K/100km/hr to the offshore frontal boundary.

By 1400 UTC the front is dividing into two distinct boundaries. First, in the northern portion of the local frontogenesis map (Fig. 4.1f), there is an area of frontogenesis with magnitudes that are slightly smaller than the previous hours. The advection term (Fig. 4.1h) is weakly frontolytic along much of the northern and offshore southern portions of the front. The confluence term (Fig. 4.1g) was the only term that was strongly frontogenetic along the North Carolina/Virginia border, with a maximum of 1°K/100km/hr. The shear term (Fig. 4.1i) is frontolytic in that same area and is weakly frontogenetic to the south.

Next, the region of the frontal breakdown near southwestern portion of Pamlico Sound is examined. The local frontogenesis map (Fig. 4.1f) depicts an area of frontolysis, with a maximum of -0.5°K/100km/hr in the area of frontal discontinuity. The advection term (Fig 4.1h) is frontolytic with a local maximum of -0.6°K/100km/hr over the center of the discontinuity. It is apparent

that the advection term is the most important contributor to frontolysis. The confluence map (Fig 4.1g) depicts a large area of weak frontogenesis over eastern North Carolina with a small area of frontolysis in the proximity the frontal discontinuity. The shear contribution (Fig. 4.1i) is only very weakly frontogenetic over eastern North Carolina with a local minima of zero over the area of frontal discontinuity.

Finally, the offshore portion of the front is examined. During this period the front has moved slightly closer to shore. Figure 4.1f depicts an area of strong frontogenesis over the front and an area of frontolysis further out to sea. In addition, the advection, confluence, and shear terms are all weakly frontogenetic over the frontal zone.

By 1500 UTC (Fig. 4.1j) the northern portion of the frontal system has reestablished itself further inland. The local frontogenesis associated with the inland front is positive with a maximum of 1°K/100km/hr· In addition, the weak "orphan front" along the coast has a corresponding frontogenetic area which is slightly stronger than during the previous few hours. There is still an area of frontolysis with a maximum of -0.9°K/100km/hr in the zone between the two fronts. Again, the advection, confluence, and shear maps all had corresponding areas of frontolysis (not shown). The advection contribution is again the largest with a maximum of -0.9°K/100km/hr. Both the confluence and the shear maps have

areas near zero in the area of frontal discontinuity.

By 1800 UTC (Fig. 4.1k) the local frontogenesis map is more characteristic of a strengthening and slow moving frontal zone. There is a strong area of frontogenesis ahead of and a strong area of frontolysis behind the inland front. The frontogenesis and frontolysis had reached maxima of 2.6°K/100km/hr and -1.2°K/100km/hr, respectively. This sharp contrast across the frontal zone is evident when examining the temperature gradient in central North Carolina where a maximum of 12.9°C/100km has become established. Also, the confluence and shear are strongly frontogenetic with each term contributing a local maximum of 1.4°K/100km/hr. To the east of the front, the confluence and shear terms are zero or slightly negative. The advection term is strongly frontolytic with a maximum of -1.9°K/100km/hr to the east of the inland front. Again, there is an area of weak frontogenesis along the coast; with roughly equal contributions from the advection, confluence, and shear terms.

In summary, as the front establishes itself over the Pamlico Sound region in eastern North Carolina early in the morning, there are corresponding areas of frontogenesis along the frontal boundary until 1400 UTC. Up to this point the front was becoming well defined. However, near 1400 UTC an area of frontolysis, largely due to advection, forms over southwest Pamlico Sound and the frontal boundary begins to break up. Two separate boundaries reform by 1500 UTC. The inland boundary is much stronger and it reformed

from the original front. The second boundary (orphan front) maintains itself over the outer banks of North Carolina. By 1800 UTC the inland front is very well developed with a sharp temperature gradient. The main frontogenetic forcing for this development is due to confluence and shear.

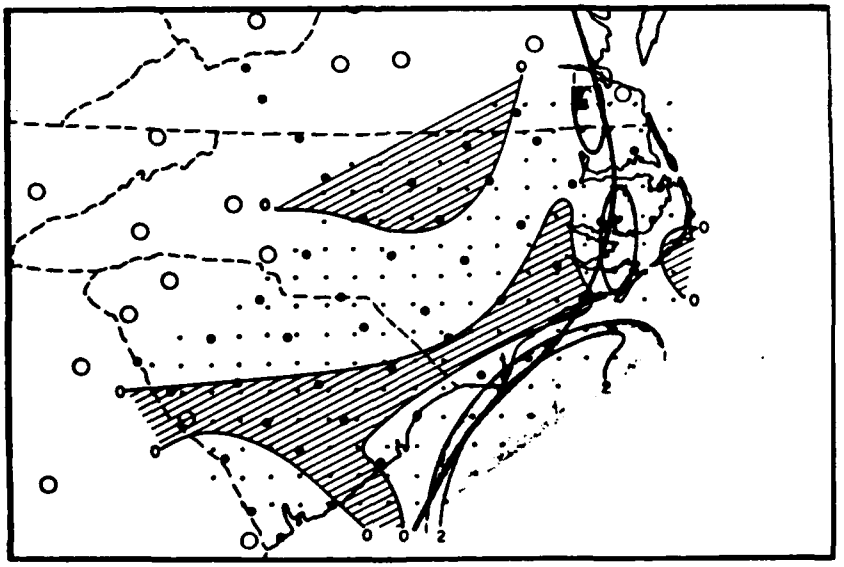

Figure 4.1a - Local frontogenesis at 1200 UTC 25 January 1986. Negative regions are represented by hatched areas. Values greater than 1°K/100 km/hour are shaded gray. The thick line is the frontal position from the surface analysis.

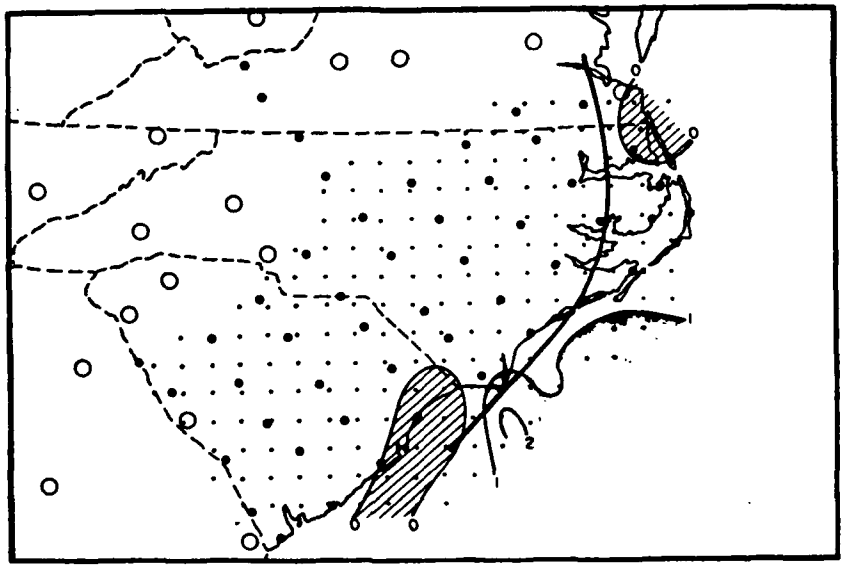

Figure 4.1b - Shear deformation at 1200 UTC 25 January 1986. Negative regions are represented by hatched areas. Values greater than 1°K/100 km/hour are shaded gray. The thick line is the frontal position from the surface analysis.

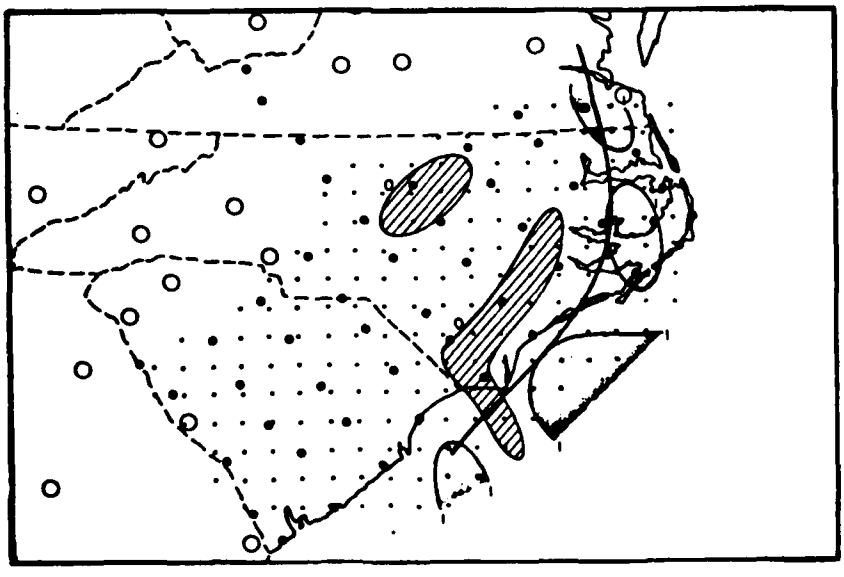

Figure 4.1c - Confluence at 1200 UTC 25 January 1986. Negative regions are represented by hatched areas. Values greater than 1°K/100 km/hour are shaded gray. The thick line is the frontal position from the surface analysis.

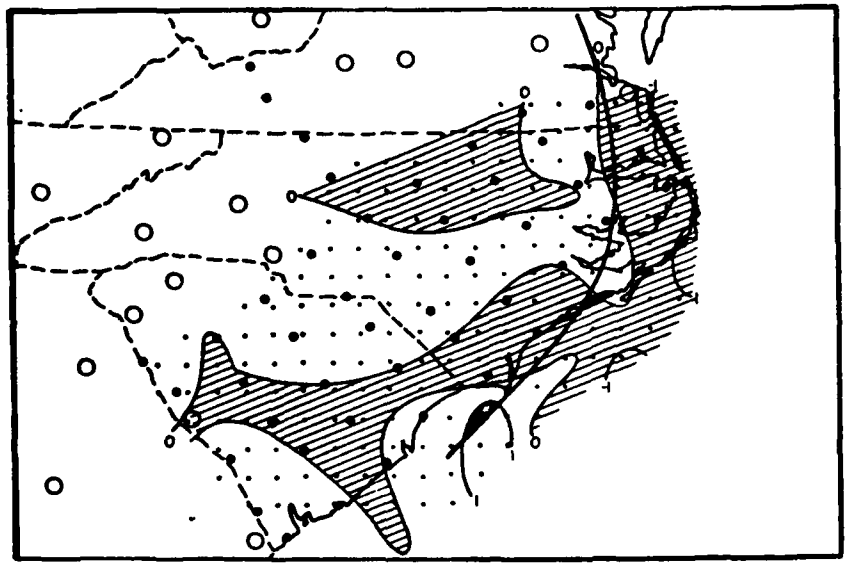

Figure 4.1d - Advection contribution at 1200 UTC 25 January 1986. Negative regions are represented by hatched areas. Values greater than 1°K/100 km/hour are shaded gray. The thick line is the frontal position from the surface analysis.

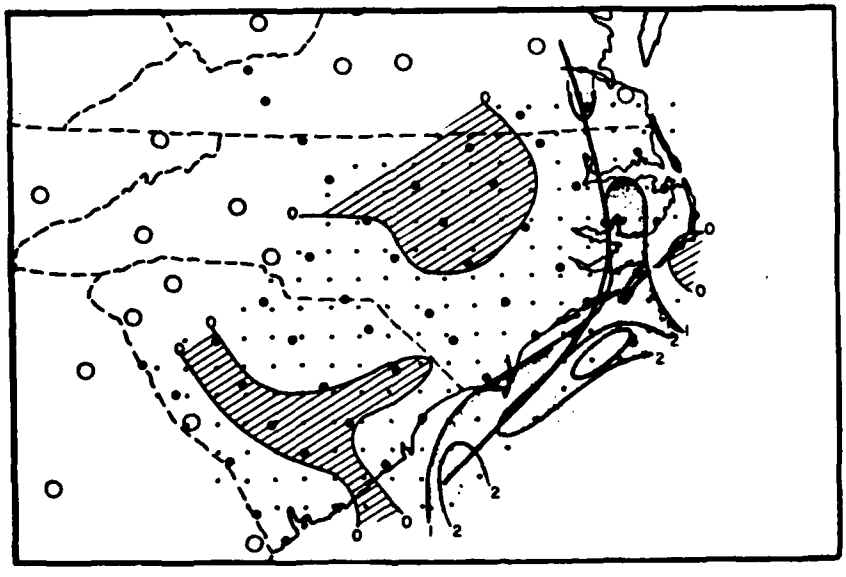

Figure 4.1e - Local frontogenesis at 1300 UTC 25 January 1986. Negative regions are represented by hatched areas. Values greater than 1°K/100 km/hour are shaded gray. The thick line is the frontal position from the surface analysis.

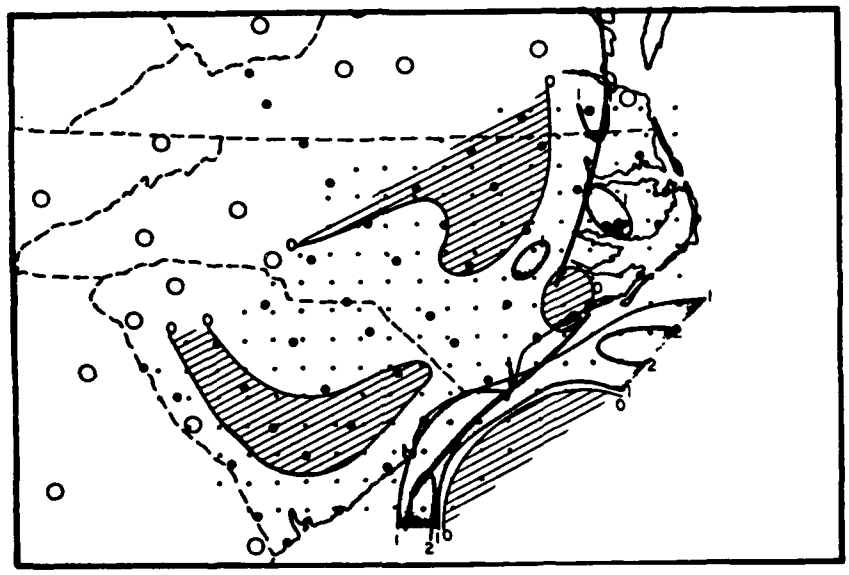

Figure 4.1f - Local frontogenesis at 1400 UTC 25 January 1986. Negative regions are represented by hatched areas. Values greater than 1°K/100 km/hour are shaded gray. The thick line is the frontal position from the surface analysis.

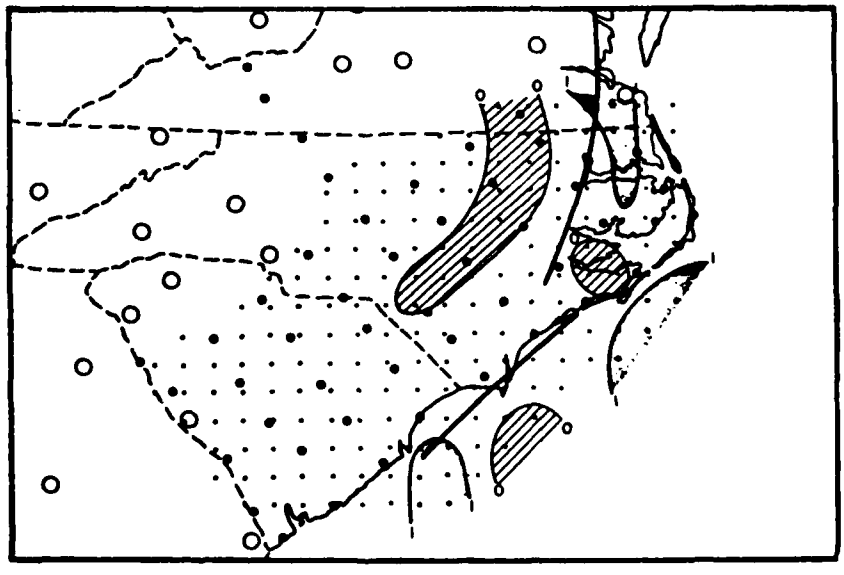

Figure 4.1g - Confluence at 1400 UTC 25 January 1986. Negative regions are represented by hatched areas. Values greater than 1°K/100 km/hour are shaded gray. The thick line is the frontal position from the surface analysis.

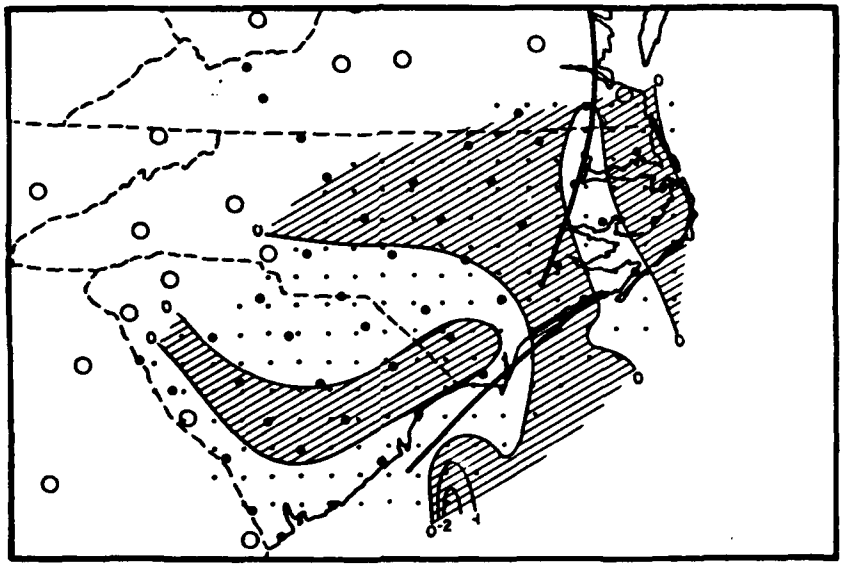

Figure 4.1h - Advection contribution at 1400 UTC 25 January 1986. Negative regions are represented by hatched areas. Values greater than 1°K/100 km/hour are shaded gray. The thick line is the frontal position from the surface analysis.

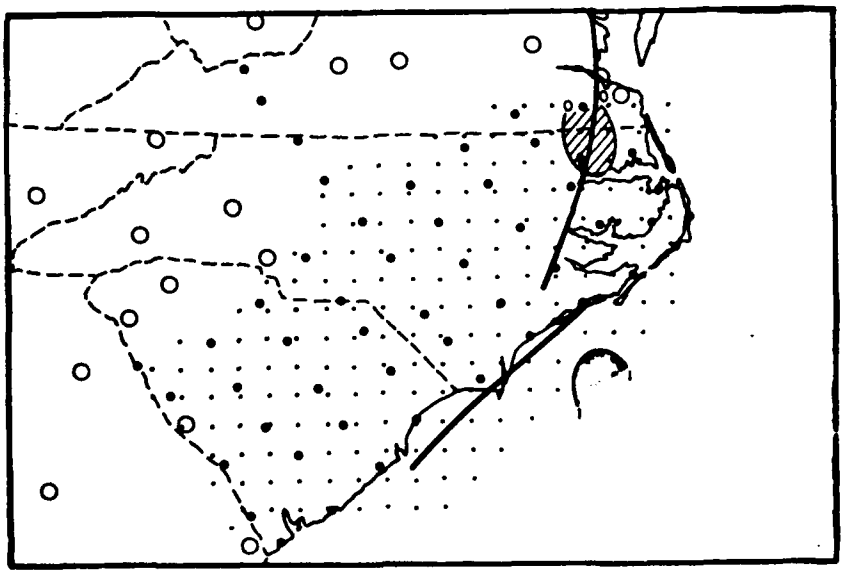

Figure 4.1i - Shear deformation at 1400 UTC 25 January 1986. Negative regions are represented by hatched areas. Values greater than 1°K/100 km/hour are shaded gray. The thick line is the frontal position from the surface analysis.

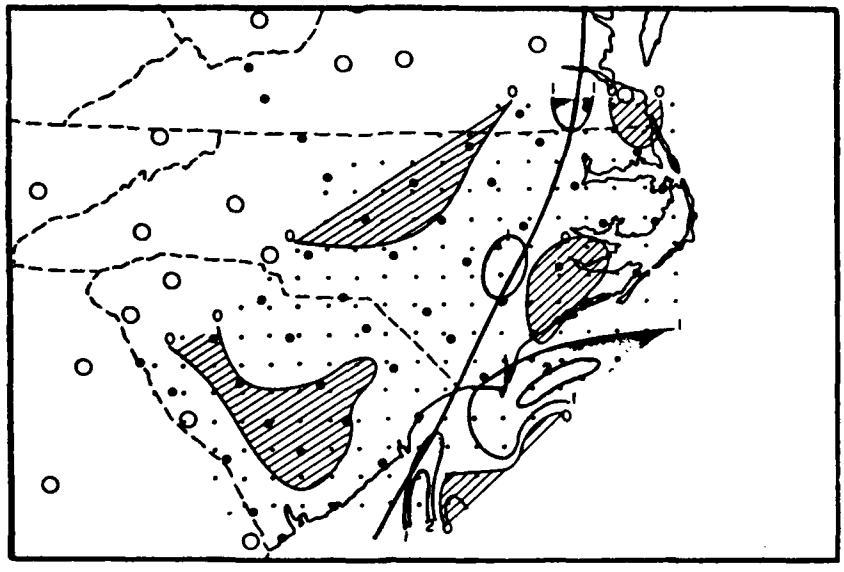

Figure 4.1j - Local frontogenesis at 1500 UTC 25 January 1986. Negative regions are represented by hatched areas. Values greater than 1°K/100 km/hour are shaded gray. The thick line is the frontal position from the surface analysis.

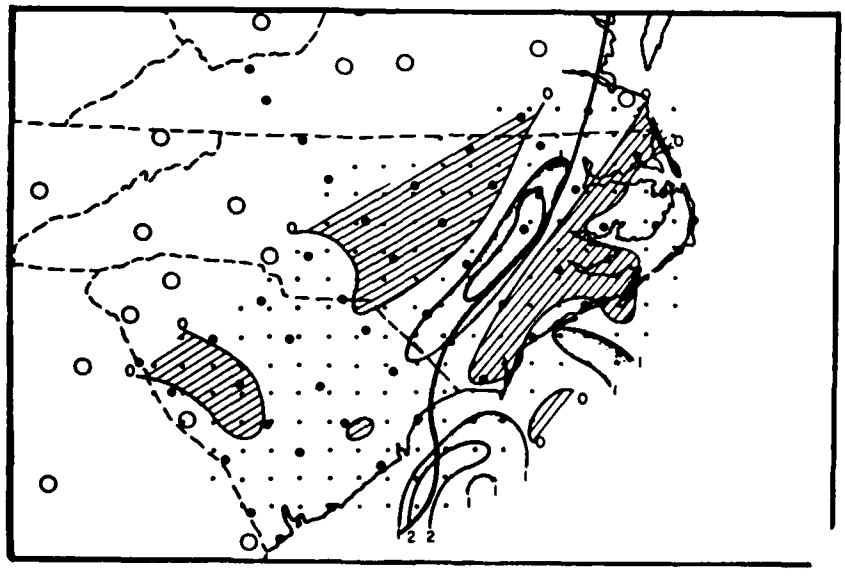

Figure 4.1k - Local frontogenesis at 1800 UTC 25 January 1986. Negative regions are represented by hatched areas. Values greater than 1°K/100 km/hour are shaded gray. The thick line is the frontal position from the surface analysis.

4.2 Error Estimate

There are several sources of potential errors in the calculations performed in this paper. Here we define 'error' as inclusion in mesoscale analysis of those measurements: 1) representative of smaller scales of motion; 2) contaminated by instrumental or siting errors. The first problem arises from the fact that both spatially and temporally, measurements at the PAM sites do not necessarily represent the mesoscale field. Even the five-minute averaged observations reveal significant 5-minute variability, evidently associated with turbulence. This variability is suppressed, but not eliminated, by the Barnes analysis; the remaining error is compounded through the frontogenetic calculations.

4.2.1 PAM Station Accuracy and Representativeness

The most basic type of error can be found in the initial measurement of the parameter of interest. The accuracy of the PAM instruments as calculated by the NCAR Field Observing Facility is given as plus or minus 0.25°C for the temperature and plus or minus 1 m/s for the wind measurements. This error is acceptable, in fact it will be seen that instrument error may be very small compared with the representativeness errors.

The errors are reduced somewhat by the shear number of measurements at each PAM site. For example, the measurements of the u and v components are taken at 1-second intervals and the

temperature measurements are taken every 10 seconds. These readings are then averaged over a 5-minute time period.

One way to estimate the magnitude of both small scale disturbances and of instrumental error and exposure biases on the PAM data is to compare PAM site 51 with Raleigh-Durham Airport (RDU). The distance between these two measuring sites is approximately 200 meters. First, a comparison between temperatures was performed. Eight days from the second month of the project were chosen at random from the GALE data set and compared to the RDU data set. Differences were then taken between the temperatures (Celsius) on-the-hour for a 24-hour period. Next, the standard deviations for each of the eight days were calculated (see table 4.2.1). The range of the standard deviations was from 0.41 to 1.51°C. If a normal distribution of standard deviations is assumed, the median value can be used to represent the error. So, the error estimate for the temperature is 0.71°C which is considerably larger than 0.25°C, suggested by NCAR.

For purposes of the frontogenetic calculations the error estimate in the wind velocity is the other variable that needs to be considered. This is difficult to evaluate because, in addition to instrument accuracy, the measurement critically depends on exposure and proximity of obstacles around the site which affect both the mean-wind and, to a greater extent, small-scale turbulence which influences 5-minute observations. One way to estimate the

wind error is by examining the components (u and v) at several different stations. Five-minute measurements from PAM site 14 and 45 are shown in figure 4.2a. Figure 4.2a depicts the wind variation at PAM site 14 (in light wind conditions) and PAM site 45 (during a much stronger wind) where sub-mesoscale variations in the zonal wind component are evident. The results are shown in table 4.2.2. The hourly averages and standard deviations for wind speeds are listed for each hour. There is a fairly wide range of standard deviations, from a low of 0.13 to a high of 1.31. Thus a standard deviation of approximately 1 m/s is adopted for the error calculations to be described.

Comparison of Temperature Between PAM Site 51 and RDU

1.51
0.76
0.51
0.46
0.66
0.90
0.41
0.92

Table 4.2.1 - Temperature comparison between PAM-II site 51 and RDU (National Weather Service). The standard deviations of random comparisons are listed.

TIME	PAM SITE 14		PAM SITE 45	
	MEAN SPD	STD DEV	MEAN SPD	STD DEV
10.0	-0.4	0.13	-7.3	0.82
11.0	-0.24	0.19	-6.49	0.75
12.0	-0.26	0.27	-6.92	0.3
13.0	-0.19	0.3	-6.19	0.33
14.0	-0.32	0.29	-6.02	0.46
15.0	-0.01	0.3	-5.44	0.67
16.0	0.19	0.21	-3.21	0.61
17.0	0.27	0.15	-2.28	1.21
18.0	0.33	0.19	-1.1	1.3
19.0	0.27	0.19	-2.03	0.66
20.0	0.33	0.27	-1.42	1.31
		0.23		0.77

Table 4.2.2 - Wind error analysis of PAM site 14 and site 45. The mean wind speed (u-component) and the standard deviation are listed for each hour. The total standard deviation for the sites are also listed.

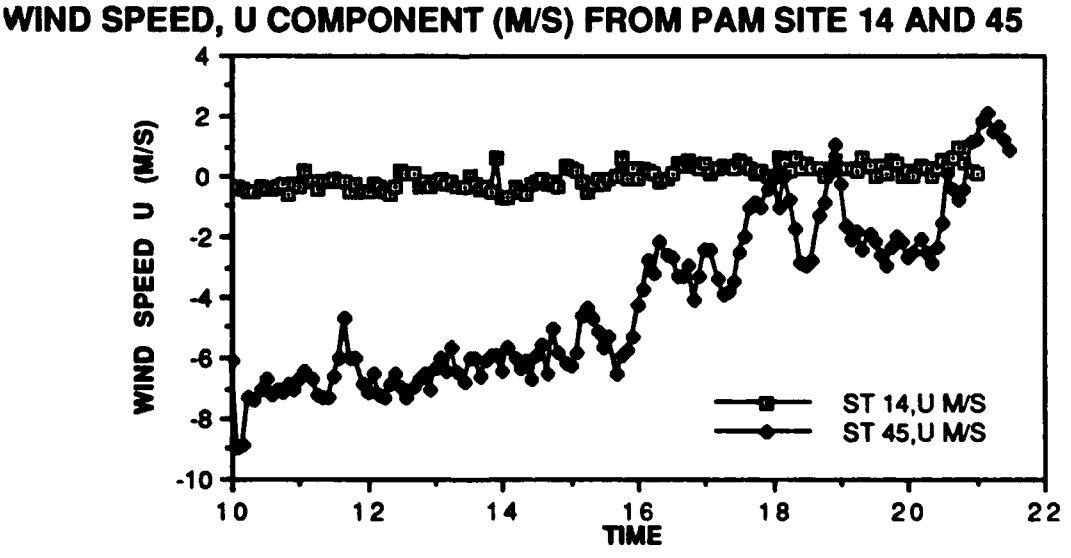

Figure 4.2.a - PAM-II site 14 and 45, wind speed (u-component) is plotted versus time for 25 January 1986.

4.2.2 Frontogenesis Error Calculations

The Barnes Analysis carries forward the errors of the temperature and wind speed because it utilizes the raw data. It replaces the scattered data points with a grid of data points. Some of the errors are smoothed out by the analysis procedure, as discussed in an earlier section. Grid point values of u, v, and T obtained by the Barnes Analysis are used to calculate the frontogenetic terms. In this case, the small errors can become large problems because the frontogenetic equations are calculated by the finite-difference method. One way to estimate the impact of the errors on the final result is by adding or subtracting random deviations to the original observations and then recalculating the quantities of interest from this new data set. This Monte Carlo experiment should be repeated several times.

First, the standard deviation of the errors at the PAM sites were determined to be 0.71°C, for the temperature, and 1 m/s, for the u and v wind components. Next, random errors were introduced into the PAM observations. These random-error-induced fields were produced by randomly adding or subtracting errors defined by a normal distribution with a mean of zero and the standard deviations given above. In this way, 30 sets of data were produced for 1800 UTC. The 30 PAM fields with the random errors were each then analyzed by the Barnes scheme and the frontogenetic processes calculated. Finally, error statistics were tabulated at each grid

point. Figure 4.3a depicts the mean local frontogenesis, figure 4.3b depicts the maximum local frontogenesis, figure 4.3c depicts the minimum local frontogenesis, and figure 4.3d depicts the standard deviation. Here, maximum and minimum values refer to the largest and smallest values, in the algebraic sense, over the 30 experiments. The maximum, minimum, and mean maps are analyzed as before with the negative areas hatched, terms greater than 1°K/100km/hour shaded gray, and the frontal position marked by the thick line. The standard deviation of local frontogenesis is analyzed every 0.1 unit.

First, the mean local frontogenesis at 1800 UTC (Fig. 4.3a) is compared to the original local frontogenesis (Fig. 4.1k). The general pattern of frontogenesis/frontolysis is the same in both maps. The strong frontogenetic area adjacent and to the west of the frontal zone is common to both maps with the mean local frontogenesis being slightly weaker (2.0°K/100km/hour) than the local frontogenesis (2.6°K/100km/hour).

A comparison of the maximum local frontogenesis (Fig. 4.3b) with the original local frontogenesis (Fig. 4.1k) again reveals that the area just to the east of the front is frontolytic and the area to the west is strongly frontogenetic. Comparison of the minimum local frontogenesis with the original local frontogenesis also gives similar results.

Finally, it is of interest to compare the maximum and minimum local frontogenesis. These two fields represent the largest

deviations induced by random error across the front. The range of values based on the 30 experiments is from -0.4 to +1.2 units. Even with the worst case scenario, the frontal boundary has local frontogenesis west of the front and frontolysis east of the front, and the uncertainty at any grid point is at or below plus or minus 1°C/100km/hour. So, the integrity of the front and frontogenesis and frontolysis patterns remains intact regardless of the errors.

The pattern of standard deviation of the 30 cases gives an overall impression of the impact of random errors. Typical values are generally about 20 percent of the mean local tendency. Hence, considerable reliability can be placed in the original calculated values at 1800 UTC.

Also the cyclonic eddy should be examined with respect to the error estimates. Specifically, the wind speed error of 1 m/s is equal to the wind at PAM site 40, in the eastern portion of the eddy, so the presence of the eddy might seem questionable. On the other hand, there is continuity in the wind direction and speed at PAM site 40 and the front breaks down in the area of the eddy. These factors indicate the eddy is present. So, at least in this case it appears the error estimates are larger than necessary.

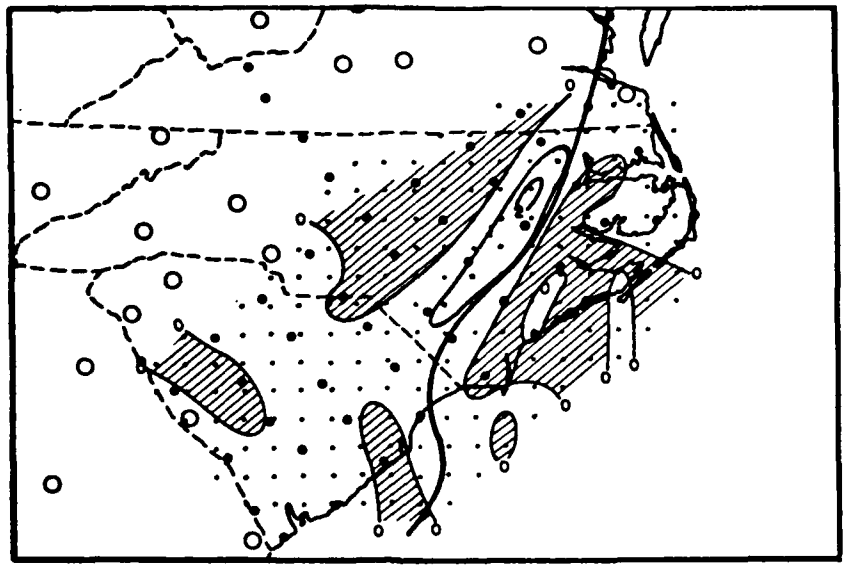

Figure 4.2a - Mean local frontogenesis at 1800 UTC 25 January 1986. Negative terms are represented by hatched areas. Values greater than 1°K/100km/hour are shaded gray. The thick line is the frontal position from the surface analysis.

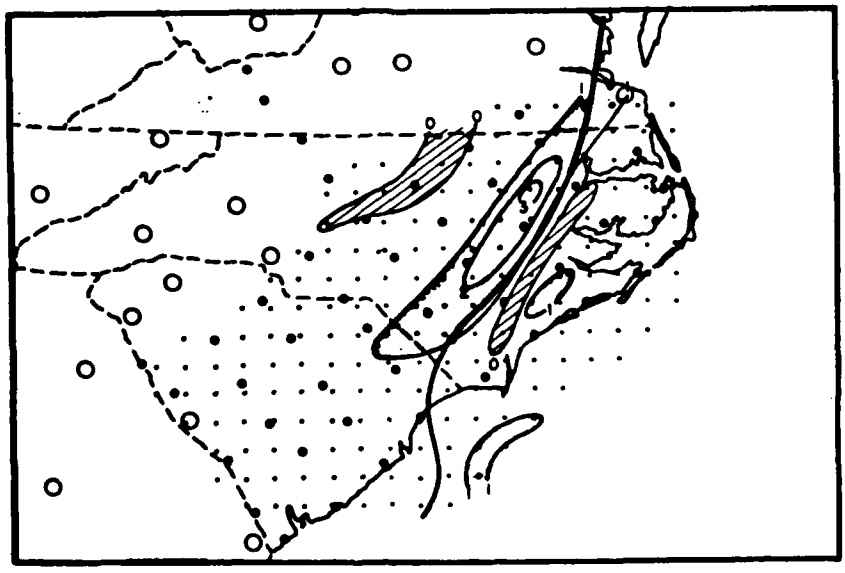

Figure 4.2b - Maximum local frontogenesis at 1800 UTC 25 January 1986. Negative terms are represented by hatched areas. Values greater than 1°K/100km/hour are shaded gray. The thick line is the frontal position from the surface analysis.

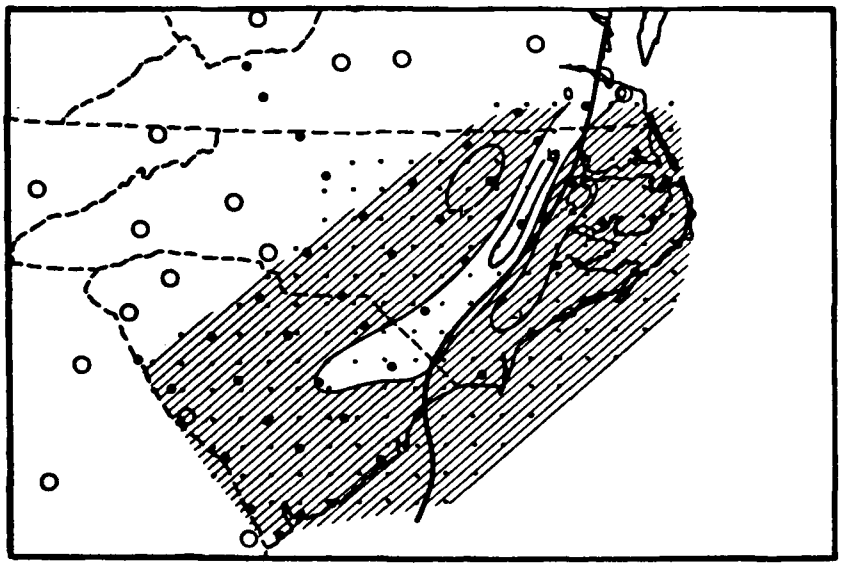

Figure 4.2c - Minimum local frontogenesis at 1800 UTC, 25 January 1986. Negative terms are represented by hatched areas. Values greater than 1°K/100km/hour are shaded gray. The thick line is the frontal position from the surface analysis.

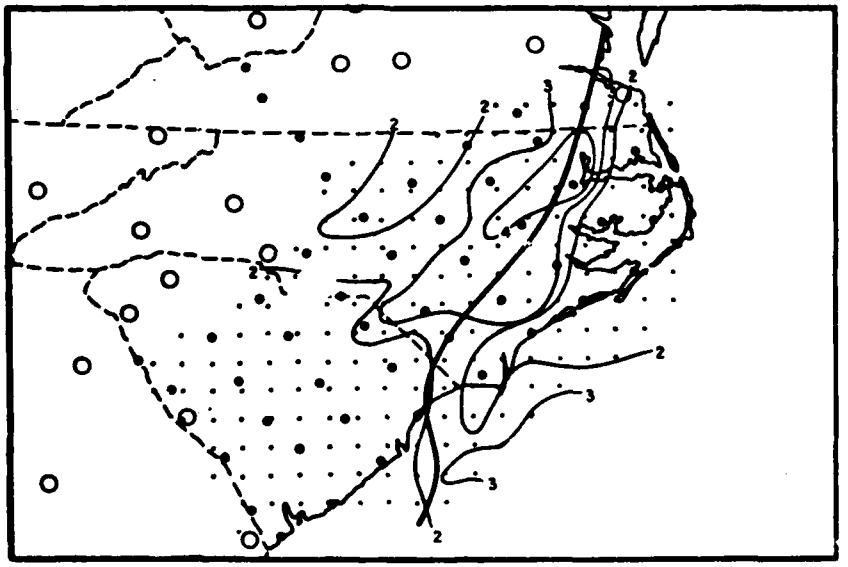

Figure 4.2d - Standard deviation of local frontogenesis at 1800 UTC 25 January 1986. The contours are analyzed every 0.1 °K. The thick line is the frontal position from the surface analysis.

5. CONCLUSIONS

The primary objectives of this study were to employ the enhanced data collection during the GALE project on 25 January 1986 to produce a mesoscale analysis of the evolution of the coastal front in eastern North and South Carolina, to explain the development of the coastal front by a numerical finite-difference evaluation of the physical processes, and to obtain an error estimate on the frontogenetic terms.

The mesoscale analysis produced some interesting results. First, the coastal front not only moves inland, but it is destroyed and reforms as two separate frontal boundaries. The separation is associated with a small cyclonic feature over southwest Pamlico Sound with an associated area of divergence at 1400 UTC. The inland front becomes stronger than the frontal remnant near shore, termed the orphan front. The latter, although weak, is a deeper system than the inland front and has a boundary sloping inland traceable to 850 mb. This relatively deep frontal remnant system may produce sufficient forcing for rainshowers, which at this time are confined to the Pamlico Sound and coastal region.

The inland frontal boundary moves farther inland throughout the period. This westward motion is likely due to: 1) turbulent mixing at the lower frontal boundary aloft; 2) superadiabatic lapse rates which suggests convective mixing along the front.

The numerical finite-difference evaluation of the individual

terms produced interesting results. Throughout the period confluence and shear are mainly responsible for the frontogenetic forcing along the main inland front. However, the cyclonic circulation in southwest Pamlico Sound, at 1400 UTC, is associated with frontolysis largely due to the advection term.

A sensitivity test of random error on the frontogenetic terms is encouraging. The frontogenesis calculations were repeated on 30 error-simulations and the overall mean pattern of frontogenesis remained constant. The worst-case maximum error scenario still resulted in the same location of the front and the areas of frontogenesis and frontolysis. Finally, the random errors are generally about 20 percent of the mean local tendency.

6. FUTURE RESEARCH

The limiting factor in studying the coastal front is the quantity of data. The GALE network improved the temporal and spatial data resolution but did not sufficiently measure the vertical structure of the shallow coastal front. The soundings used during GALE ascended too fast and thus recorded limited observations in the lower few hundred meters, missing the shallow coastal front. In addition, the IOP did not begin until the coastal front was established, so there is limited time resolution of the data. A new way to collect data for the vertical profile of the coastal front must be developed. The amount of data collected can be increased by using tethersondes or using slower-ascent balloons for the soundings.

The future research of the coastal front should include methods to measure or estimate the diabatic heating, so one could perform a more complete frontogenesis evaluation.

Also, a climatological study can be performed to determine, for example, whether the cyclonic circulation found in the southwest Pamlico Sound region or the frontal breakdown into the inland and orphan coastal fronts are features common to all coastal fronts that move onshore in the Carolinas.

REFERENCES

Ballentine, R.J., 1980: A numerical investigation of New England coastal frontogenesis. Mon. Wea. Rev., 108, 1479-1497.

Barnes, S.L., 1964: A technique for maximizing details in numerical weather map analysis. J. Appl. Meteor., 3, 396-409.

___, 1973: Mesoscale objective analysis using weighted time-series observations. NOAA Technical Memorandum ERL NSSL-62, Norman, OK., 60 pp.

___, 1985: Omega diagnostics as a supplement to LFM/MOS guidance in weakly forced convective systems. Mon. Wea. Rev., 113, 12, 2122-2141.

Bejerknes, J., 1919: On the structure of moving cyclones. Geofys. Publ., 1, 1-8.

___, 1932: Explorations de quelques perturbations atmospheriques a l'aide de sondages rapproches dans le temps. Geofys. Publ., 9, No. 9.

___, and E. Palmen, 1937: Investigations of selected European cyclones by means of serial ascents. Geofys. Publ., 12, No. 2.

Bosart, L.F., C.J. Vaudo and J.H. Helsdon, Jr., 1972: Coastal frontogenesis. J. Appl. Meteor., 11, 1236-1258.

___, 1975: New England coastal frontogenesis. Quart. J. Roy. Meteor. Soc., 101, 957-978.

___, 1981: The president's day snowstorm of 18-19 Febuary 1979: A Subsynoptic Scale Event. Mon. Wea. Rev., 109, 1542-1566.

___, and Lin S.C., 1984: A diagnostic analysis of the presidents' day storm of Febuary 1979. Mon. Wea. Rev.,112, 2148-2177.

Carson, R.B., 1950: The Gulf Stream front: A cause for stratus on the lower Atiantic coast. Mon. Wea. Rev., 78, 91-100.

Diaconis P. and Efron B.k, 1983: Computer-intensive methods in statistics. Sci. Amer., 248, 5, 116-130.

Dirks, R.A., J.P. Kuettner, and J.A. Moore, 1988: Genesis of Atlantic Lows Experiment (GALE): An Overview. Bull. Amer. Meteor. Soc., 69, 148-160.

George, J.J. 1939: The causes and forecasting of low ceilings and fog at the Jacksonville Airport, Eastern Air Lines, Atlantic, Ga.

Haltiner, G.J., and F.L. Martin, 1957: Dynamical and physical meteorology. McGraw-Hill, 287-296.

Holton, J.R., 1979: An Introduction to Dynamic Meteorology 2d ed. Academic Press, 391 pp.

Hoskins, B.J. and F.P. Bretherton, 1972: Atmospheric frontogenesis models: mathematical formulation and solution. J. Atmos. Sci., 29, 11-37.

Marks, F.D. and P.M. Austin, 1979: Effects of the New England coastal front on the distribution of precipitation. Mon. Wea. Rev., 107, 53-67.

Miller, J.E., 1948: On the concept of frontogenesis. J. Meteor., 5, 169-171.

Moore, J.T., and P.D. Blakley, 1988: The role of frontogenetical forcing and conditional symmetric instability in the midwest snowstorm of 30-31 January 1982. Mon. Wea. Rev., 116, 8, 2142-2154.

Namias, J., and P.F. Clapp, 1949: Confluence theory of the high

tropospheric jet stream. J. Meteor., 6, 330-336.

Newton, C.W., 1954: Frontogenesis and frontolysis as a three-dimensional process. J. Meteor., 11, 449-461.

Nieuwstadt, F.T.M., and H. von Dop, 1982: Atmospheric Turbulence and Air Pollution Modelling. Atmospheric Sciences Library, 358 pp.

Palmen, E. and C.W. Newton, 1969: Atmospheric Circulation Systems. Academic Press, 603 pp.

Pettersen, S., 1940: Weather Analysis and Forecasting. McGraw-Hill, 505 pp.

Richwein, B.A., 1980: The damming effect of the southern Appalachians. Nat. Wea. Dig., 5, 2-12.

Riordan, A.J., S. SethuRaman, J.M. Davis, and S. Viessman, 1985: Measurements in the marine boundary layer near a coastal front. Geophy. Res. Let., 12,10, 681-684.

Riordan, A.J., 1989: Examination of the mesoscale features of the GALE coastal front of 24-25 January 1986. Mon. Wea. Rev. in review.

Saucier, W.J., 1955: Principles of Meteorological Analysis. University of Chicago, 438 pp.

Schwerdtfeger, W.E., 1973: Mountain Barrier Effects on the Stable Air North of the Brooks Range. Climate of the Arctic, 204-208.